Phylogeny of *Weinmannia* (Cunoniaceae) reveals the contribution of the Southern Extratropics to Tropical Andean biodiversity

Ricardo A. Segovia*[1], Eduardo Aguirre-Mazzi*[2,3], Christine E. Edwards[3], Alexander G. Linan[3], Alfredo Fuentes[3,4], Andrea Chaspuengal[5], Kyle G. Dexter[6,7], Francisco Fajardo-Gutiérrez[8], William Farfan-Rios[9], Nora H. Oleas[5], Juan C. Penagos Zuluaga[10], J. Sebastián Tello[3]

Abstract

The Andes are a relatively young mountain range with impressive biodiversity, but the biogeographic processes underlying its hyperdiversity are still being unraveled. Novel mid- to high-elevation climates may have served as a biological corridor for the immigration of temperate-adapted lineages to more equatorial latitudes, contributing unknown levels of diversity to this region. We tested the hypothesis that *Weinmannia* is a lineage of extratropical origin that recently reached and then diversified extensively in the tropical Andes. Using a 2bRAD seq approach to generate a time-calibrated phylogeny for the genus, we found that extratropical species were placed as sister to the rest of *Weinmannia* and that younger clades were distributed towards more equatorial latitudes. Although *Weinmannia* exhibited low niche conservatism in elevation and latitude, trait reconstructions of climatic variables showed that the common ancestor of *Weinmannia* occupied cool climates, with high conservatism of thermal and water availability niche across the phylogeny. Thus, Andean uplift likely created habitats with suitable environmental conditions, providing a dispersal route for extant *Weinmannia* to colonize the tropical Andes from the southern extratropics. These southern lineages likely converged with those originating in other tropical and extratropical centers of diversification, providing multiple origins for the hyperdiversity in the modern montane forests of the tropical Andes.

[1]Departamento de Botánica, Universidad de Concepción and Institute of Ecology and Biodiversity, Chile; [2]Department of Biology, Washington University in St. Louis, St. Louis, MO, United States; [3]Missouri Botanical Garden, St. Louis, MO, United States; [4]Herbario Nacional de Bolivia, Instituto de Ecología, Universidad Mayor de San Andrés, La Paz, Bolivia; [5]Centro de Investigación de la Biodiversidad y Cambio Climático (BioCamb) y Facultad de Ciencias del Medio Ambiente, Universidad Tecnológica Indoamérica, Ambato 180103, Ecuador; [6]School of GeoSciences, University of Edinburgh; [7]Royal Botanic Garden Edinburgh; [8]Botanischer Garten und Botanisches Museum Berlin-Dahlem, 14195 Berlin, Germany; [9]Department of Biology and Andrew Sabin Center for Environment and Sustainability, Wake Forest University, Winston-Salem, NC 27106, USA; [10]Yale School of the Environment, Yale University. 195 Prospect Street, New Haven, CT.

* These authors contributed equally to this work

Corresponding author; e-mail: rsegovia@ieb-chile.cl; christine.edwards@mobot.org

Keywords: immigration, diversification, hyperdiversity, tropics, Gondwana

1. Introduction

The Andean region of tropical America has one of the world's highest levels of species richness (Balslev, 1993), taxonomic endemism (Myers et al., 2000) and phylogenetic diversity (Tietje et al., 2023). This hyperdiversity is particularly intriguing given that the modern geomorphology of this area is no older than the late Miocene (< 11 Ma) (Gregory-Wodzicki, 2000; Siravo et al., 2018). Mountain building is generally thought to have fostered high diversity both through speciation of resident lineages (Rahbek et al., 2019) and the immigration of lineages pre-adapted to newly created climatic conditions (Donoghue, 2008, Linan et al., 2021a). Indeed, the Andean orogeny may have increased the rate of lineage diversification (Antonelli and Sanmartin, 2011) and may also have opened a corridor for the immigration of temperate lineages into the equatorial latitudes of the Americas (Graham, 1973; Segovia and Armesto, 2015). Comprehensive evolutionary evidence is still being gathered to identify areas of lineage origin and thus unravel the relative influence of these biogeographic processes in shaping the modern pattern of hyperdiversity in the Andes.

Phylogenetic evidence shows faster-than-expected rates of diversification for several potentially resident plant clades in synchrony with the Andean uplift since the early Miocene (e.g., Luebert and Weigend, 2014; Pérez-Escobar et al., 2022). Moreover, a growing body of phylogenetic evidence shows immigration from both the northern and southern extratropics into the tropical Andes. Many lineages have immigrated from the northern extratropics, including *Viburnum* (Winkworth and Donoghue, 2005), *Lupinus* (Hughes and Eastwood, 2006), and *Passiflora* section *Decaloba* (Achá et al., 2021). There is also evidence of lineages immigrating from the southern extratropics, including Geraniales (Palazzesi et al., 2012), Alstroemeriaceae (Chacón et al., 2012), *Podocarpus* (Quiroga et al., 2016), *Gunnera*

(Bacon et al., 2018), and Loranthaceae (Liu et al., 2018). However, most of what we know about these biogeographic scenarios for the origin of the plant diversity in the tropical Andes has disproportionately focused on taxa inhabiting open biomes at high-elevations. Evidence regarding the origin and direction of dispersal routes of the clades that occupy montane forests at intermediate elevations remains scarce, representing a significant gap in our understanding of plant diversity and evolution in one of the most species-rich regions on the planet.

The notion that lineages from the extratropics, which are presently species-poor, could have contributed to the present-day hyperdiversity of the tropical Andes seems counterintuitive. Traditionally, the highest levels of species richness are thought to be associated with "centers of diversification" (Willis, 1922), or areas where a particular lineage originated (Wiens and Donoghue, 2004), and there is strong evidence that the American tropics have historically acted as a "species pump" for global plant diversity (Antonelli et al., 2015). However, immigration from multiple zones, including the extratropics, into tropical Andean forests has been identified based on taxonomic affinities (Hooghiemstra, 1984), fossil records (Graham, 1995), and community phylogenetics (González-Caro et al., 2023), not just through clade reconstructions. These multi-source immigration processes, along with rapid lineage diversification, may be key to shaping the modern hyperdiversity of the tropical Andes, increasing not only taxonomic diversity but also evolutionary diversity, according to the "environmental crossroads hypothesis" (Neves et al., 2020; Griffiths et al., 2021). For example, the exceptionally high phylogenetic diversity found in the central and northern Andes (Tietje et al., 2023) may be due to the mixing of deeply isolated communities with different evolutionary histories (e.g., remnants of paleobiota from the Holarctic, Austral and Neotropical floristic realms).

Here we investigate the biogeography of *Weinmannia* L. (*sensu* Pillon et al., 2021), Cunoniaceae, formerly *Weinmannia* sect. *Weinmannia* L. (Bradford, 1998), an important genus of trees and shrubs in Andean forests given their high abundance and diversity. Typically considered an extratropical southern hemisphere taxon (Raven and Axelrod, 1974), *Weinmannia* comprises two species occurring in the Mascarenes (Indian Ocean) and over 90 species in the Americas (Bradford, 1998, 2002; Pillon et al., 2021). Most *Weinmannia* species occur at mid- to high-elevations (> 1500 m) in the montane forests of the tropical Andes, where they exhibit overlapping morphologies due to either recent divergence or hybridization (Bradford, 1998, 2002). In addition, several species occur in the Guiana Shield and mountain peaks of Central America and the Caribbean Islands. Three species are endemic to the subtropical forests of eastern Brazil (i.e., Mata Atlantica), and one species occurs in the temperate forests of southern South America (Chile and Argentina). Previous phylogenies placed the only southern extratropical species (*Weinmannia trichosperma* Cav.) as an early diverging lineage of *Weinmannia* (Bradford, 1998, 2002), sparking the hypothesis that *Weinmannia* immigrated into the tropics from the southern extratropics following the Andean uplift (Bradford et al., 2004; Pennington and Dick, 2004). However, these analyses sampled only a small proportion of the species (< 6 species) in the genus (Bradford, 2002; Pillon et al., 2021) and employed only a small number of plastid and/or nuclear regions (Bradford, 2002), limiting their ability to provide support for hypotheses about the origin and dispersal of *Weinmannia* throughout the Andes.

To examine the hypothesis of a southern extratropical origin for *Weinmannia* and its recent immigration into the tropical Andes, we reconstructed a new NGS phylogeny with dense taxon sampling. First, we tested the prediction that if the genus *Weinmannia* originated in the southern extratropics, *W. trichosperma* from the temperate forests of southern South America should be resolved as the sister lineage to all other American *Weinmannia* species. Second, we tested the prediction that if the modern distribution of *Weinmannia* in the Americas is a consequence of dispersal from the southern extratropics into the tropical Andes, the ages of nodes in the phylogeny should show a negative relationship with the reconstructed latitude of the nodes. In other words, the phylogeny should show a pattern in which younger clades occupy successively more northern latitudes. Additionally, based on ancestral character estimation, we explored patterns of evolution in the climatic niche of *Weinmannia* and tested whether it reflects phylogenetic conservatism in environmental preferences of lineages originating from extratropical climates.

2. Materials & Methods

2.1. Sampling and genomic DNA extraction. We collected 896 samples, representing 46 of the 75 (Ulloa-Ulloa et al., 2017) to 90 (Pillon et al., 2021) *Weinmannia* species estimated to occur in the Americas. These samples were collected throughout South America, including the southern Andes (Chile), central Andes (Bolivia and southern Peru) and northern Andes (Ecuador and Colombia), although central and northern Peru were not sampled due to logistical constraints. We also included four samples of two species occurring in the Mascarene Islands. For each sample, we preserved leaf tissue in silica and collected a herbarium voucher specimen. In addition, we included five specimens from three species of *Pterophylla* D.Don (*sensu* Pillon et al., 2021) as outgroups.

To extract DNA, silica-dried tissues were ground and cleaned using up to three sorbitol washes following Inglis et al. (2018) to remove mucilage and other secondary compounds. Genomic DNA was extracted using a modified CTAB extraction protocol for plants (based on Doyle and Doyle, 1987), with additional ethanol washes of precipitated DNA. Following extraction, DNA was purified using KAPA pure Beads (KAPA Biosystems) following manufacturer protocols. DNA concentrations were quantified using a Qubit™ fluorometer (ThermoFisher).

2.2. Sequencing. RAD-seq libraries were prepared using a 2b-RAD approach (Wang et al., 2012) following previously published protocols (Linan et al., 2021b; Mashburn et al., 2023). We digested 500 ng of purified genomic DNA of each sample using the BcgI restriction enzyme (New England Biolabs), producing 36 bp DNA fragments from across the genome. To ensure adequate sequence coverage per locus, 5′-NNG-3′ selective adapters were used, decreasing the number of sequenced loci (Wang et al., 2012). Using dual indexing, 96 samples were pooled per plate, whereby the first index was applied across columns, allowing pooling of the 8 rows. Each of these pools was amplified for 14 cycles of PCR while incorporating the second index (one of eight unique 6 bp Illumina TruSeq barcodes) using high-fidelity Phusion PCR mix (New England Biolabs). The amplicons were visualized using 2% Agarose gel electrophoresis and purified using the MinElute gel purification kit (Qiagen). The purified ligation pools were quantified using a Qubit fluorometer, pooled in equimolar proportions (Qiagen), and sequenced on an Illumina HiSeq 4000, generating 50 bp single end reads at the NUSeq Core facility of Northwestern University.

2.3. RAD locus assembly. Sequences were demultiplexed and trimmed to remove row and column indexes using the trim2bRAD_2barcodes.pl script (https://github.com/z0on/2bRAD_denovo). Trimmed reads were assembled *de novo* in the ipyrad v. 0.9.90 pipeline (Eaton and Overcast, 2020). To determine the optimum clustering threshold, we iterated clustering threshold within samples

(CTWS) and among samples (CTAS) using every combination of values of 0.86, 0.89, 0.92, and 0.94. The resulting matrices were compared for cluster depth, heterozygosity, the amount of putatively paralogous loci, and the number of SNPs to identify parameters that could lead to assembly errors (Paris et al., 2017). We selected a value of 0.92 for both CTWS and CTAS. All loci showing gaps or more than five SNPs were removed.

2.4. Identification of putative hybrids. To identify putative hybrid individuals that may confound phylogenetic analysis, we assessed admixture using STRUCTURE v. 2.3.4 (Pritchard et al., 2000) as implemented in ipyrad v. 0.9.90. Due to the large number of samples and putative species, we divided samples into two geographically structured datasets (central Andes region and northern Andes region), given that interspecific gene flow is most likely to occur among species with overlapping geographic ranges. For each of these datasets, we conducted an independent assembly, removing a total of 194 of 896 individuals with more than 80% missing sites, retaining loci present in at least 50% of samples, and retaining one SNP per locus. STRUCTURE analyses were run, testing values of K=2–20 with a burn-in of 300,000 generations, a run length of 700,000 generations, and 15 replicates of each K value. The optimal K value was selected using the Evanno's method (Earl and von Holdt, 2012). We defined putative hybrids as individuals with <85% assignment to a single genetic cluster, adopting a more conservative criterion compared to the 80% cut-off used by Owusu et al. (2015) and Linan et al. (2021b). A total of 337 of the 702 individuals showed signatures of hybridization according to this preliminary analysis, leaving us 365 individuals for phylogenetic analysis.

2.5. Individual-level tree inference. For phylogenetic inference, we chose 3–5 individuals with no signature of hybridization from each species, resulting in 234 accessions from 48 *Weinmannia* taxa (including 7 that are not assigned to any described species), plus 3 *Pterophylla* species that served as outgroups (total=51 species). Sequences for these specimens are available in the NCBI Sequence Read Archive (SRA) under BioProject accession PRJNA1237785.

Maximum likelihood (ML) phylogenetic analysis was conducted using a concatenated dataset of the 36 bp loci, including invariant characters. First, we performed a preliminary analysis to explore the effect of missing data on the resulting topologies, varying the percentage of samples at which a locus must be present from 4%–48% in increments of 4. We found optimal branching resolution and bootstrap support when all loci were present in at least 36% (84/234) of samples, which was used in the final analysis. The ML phylogeny was inferred in RAxML v. 8.2.12 (Stamatakis, 2014) using a rapid hill climbing algorithm and the GTRCAT approximation. Clade support was calculated using the transfer bootstrap approach with 200 iterations (Lemoine et al., 2018).

2.6. Species-level *Weinmannia* phylogeny. To reconstruct a species-level phylogeny, we selected one representative individual from each species (*i.e.*, a reciprocally monophyletic group of morphological distinctive individuals) in the individual-level phylogeny (Fig. 1A, Supplementary Fig. 1). We chose the non-admixed individual (as indicated by STRUCTURE) with the least missing data. For phylogeny reconstruction, we employed both a maximum likelihood (ML) analysis of the concatenated loci and SVDQuartets, which is a multi-species coalescent-based approach (Chifman and Kubatko, 2014). The species-level ML analysis used the same settings as described for the individual-level phylogeny. After preliminary analysis to explore the effect of missing data, we prepared a concatenated alignment of all loci present in at least 32% (16/51) of all individuals, which was used to infer a phylogeny in RAxML. The multi-species coalescent-based phylogenetic inference was performed in PAUP* (Swofford, 2002) using a randomly selected SNP from each of the 2,879 loci used in the RAxML analysis. We inferred all 249,900 possible quartets for 51 taxa and conducted 500 bootstrap iterations. The quartet trees were joined into a super tree. Branch lengths for this topology were estimated in RAxML using the same alignment as in the ML phylogeny, with the -g option to constrain the topology. Finally, we calculated bootstrap support (BS) for nodes using a transfer bootstrap approach (Lemoine et al., 2018). For visualization, the resulting trees were rooted on the branch containing all *Pterophylla* specimens.

2.7. Time-calibrated phylogeny. We inferred node ages for both our ML and SVDQ trees using treePL (Smith and O'Meara, 2012), which relies on branch length information to estimate divergence times under phylogenetically penalized likelihood, following Maurin (2008). Optimal parameters for treePL were first explored using the *prime* option. Then the optimal smoothing parameter (0.00001) was selected via random subsample and replicate cross-validation (*randomcv*), where smoothing values were tested across multiple orders of magnitude (*cvstart* = 100000 to *cvstop* = 1e-12), decreasing by a factor of 0.1 (*cvmultstep* = 0.1) over five iterations (*cviter* = 5). The best value was chosen based on minimizing predictive error as recorded in the cross-validation output. Divergence time confidence intervals were calculated through a bootstrap analysis in RAxML, constraining topology with the ML tree (-g) and optimizing branch lengths (-k) over 200 bootstrap iterations. These bootstrap trees were time-calibrated using the same treePL parameters as the ML tree. A consensus tree was generated in TreeAnnotator v.2.5.2 (Drummond and Rambaut, 2007) using the estimated and bootstrap trees, with 0% burn-in and median heights.

Three calibration points were defined for divergence time estimation. The first was a *Weinmannia* pollen fossil collected from the northern Andes of Colombia dated to ~3 million years ago (Ma) (Van Der Hammen et al., 1973). This age was defined as the minimum age for the most recent common ancestor of the clade that encompassed all specimens collected in the Northern Andes. The second point was derived from a fossil pollen record of *Weinmannia potosina* (Britton) Berry from Potosí, Bolivia from 13.8 Ma (Berry, 1917; Graham et al., 2001), which was established as the minimum age for the most recent common ancestor (MRCA) of the clade containing all Central and Northern Andean *Weinmannia* species. The upper limit for this point was set at 33 Ma, aligning with the proposed beginning of the Oligocene and previous estimates for the stem node of *Weinmannia* at 32.3 Ma (Pillon et al., 2021). Additionally, we used the 95% credibility interval with a minimum age of 29.99 Ma and a maximum age of 34.4 Ma, with a uniform distribution from Pillon et al. (2021), to estimate the divergence time between *Weinmannia* and its sister genus *Pterophylla.*

2.8. Testing biogeographic hypotheses. To test our hypothesis that *Weinmannia* migrated from south to north, we performed an ancestral reconstruction of latitude using our time-calibrated species-level phylogeny. We determined the minimum and mean latitude for each species in the phylogeny based on geo-referenced occurrence data from herbarium specimens. Ancestral character estimation was conducted using the ‘anc.ML’ function in the phytools v. 2.4.4 R package (Revell, 2024). This method was chosen because, unlike Bayesian approaches (e.g., BEAST), phytools does not require computationally intensive MCMC sampling or prior specification, making it faster and less sensitive to prior misspecification which could be exacerbated by our limited number of taxa. Additionally, it explicitly models evolutionary processes, avoiding the unrealistic assumptions of parsimony-based methods, while offering built-in functionality for exploring different trait evolution models and easy visualization tools (Revell, 2012). We compared the fit of the

Brownian motion and Ornstein-Uhlenbeck models with the Akaike Information Criterion (AIC) (data not shown), selecting the Brownian motion for all subsequent analyses due to its better fit to the data. Ancestral reconstruction of both minimum and mean latitude was performed on a pruned phylogeny without outgroups. For hypothesis testing, we performed the analysis both with and without the two Mascarene species to assess the effect of these taxa (with the pruned dataset including a total of 46 South American species). We report only the minimum latitude results here, as the mean latitude estimates were equivalent, but less reliable due to insufficient records for some species. Node ages were extracted from the time-calibrated phylogeny using the 'node.depth.edgelength' function in the ape v. 5.0 R package (Paradis and Schliep, 2019). Using data from the ancestral reconstruction, we modeled the age of hypothetical ancestors (nodes) as a function of their estimated latitudes using two distinct statistical approaches: a Bayesian approach and a frequentist approach based on a Null-Hypothesis Significance Test and non-parametric bootstrapping.

2.9. Bayesian regression analysis. We developed a hierarchical Bayesian linear regression to assess correlation structures from nesting patterns between phylogenetic nodes, considering evolutionary relationships in latitude observations. Unlike traditional approaches such as PGLS, which assess relationships between extant taxa, we tested the hypothesis that older ancestors are linked to more southern latitudes (*i.e,* more negative values), leading to a negative slope (*i.e.*, $\beta<0$ to reject the null hypothesis of $\beta\approx0$, implying no clear relationship), while accounting for non-independence of ancestral nodes through the incorporation of a node-wise variance-covariance matrix. To the best of our knowledge, no existing phylogenetic regression method supports this ancestor(node)-oriented analysis explicitly. The model was fitted using four independent MCMC chains, each running 3,000,000 iterations. For efficiency, chains were thinned every 10 iterations, yielding 300,000 samples per chain, with the first 50,000 discarded as burn-in. The max_tree depth was set to 10 to address divergent transitions during sampling. We assessed model adequacy with a posterior predictive check, comparing predicted node ages to observed data (Fig. 3B, Supplementary Fig. 5B). MCMC performance was evaluated using Gelman-Rubin statistics (Rhat), effective sample size, and autocorrelation analysis (Appendix 1 and 2). We extracted the posterior probability distribution of the slope parameter (β), along with 95% and 99% credibility intervals, and determined the maximum *a posteriori* estimate. The model code, implemented in Stan v. 2.18.2 (Carpenter et al., 2017) and executed in R using the rstan package v. 2.26.23 (Stan Development Team 2023), is provided in Appendix 3 and detailed explanation of model equations and parameters is provided in Supplementary Methods.

2.10. Non-parametric bootstrap Null Hypothesis Significance Test (NHST). To support the results of our Bayesian regression, which accounts for phylogenetic non-independence among nodes via a node-wise variance-covariance matrix, we implemented a non-parametric test that breaks phylogenetic structure through resampling. We used the glm function from the R package stats v. 3.6.2 (R Core Team 2023) to model node age as a function of reconstructed ancestral latitude under a linear regression framework. To find the model with the highest adequacy and fit, we tested combinations of two probability distributions (Gaussian and Gamma) and three link functions (identity, log and inverse) and selected the model with the lowest AIC value, highest linearity of predicted *vs* observed values (using qqplots) and better homoscedasticity. For both the ML tree and SVDQ tree-based analyses we selected gamma-distributed error and the identity function (Appendix 4 and 5). We performed a bootstrap analysis within the NHST framework with 10,000 iterations. In each iteration, we randomized reconstructed node latitudes and conducted regressions to obtain the slope parameter (β). This generated a null distribution for the slope. Because the observed slope was negative, we calculated the *p*-value as the proportion of the null distribution less than or equal to the observed slope.

2.11. Test of climatic niche conservatism. To test the hypothesis that *Weinmannia* had an extratropical origin and migrated from south-to-north as the Andean uplift created a corridor of suitable habitats, we assessed climatic niche conservatism across the phylogeny. We performed ancestral reconstructions of 19 climatic variables (BIO1 – BIO19) and elevation using our time-calibrated ML species-level phylogeny. Climatic variable values were extracted from WorldClim 2 (Fick and Hijmans, 2017) at 0.5 arc-second resolution, and elevations were estimated from geocoordinates of herbarium specimens. To evaluate trait conservatism, we used a color gradient to map observed and reconstructed values onto the species-tree edges with the 'contMap' function in phytools v.2.1, under a Brownian motion model. Using reconstructed values of 19 climatic variables, Elevation, and Latitude, we calculated the darwin (d) rate of trait evolution per unit of time (Haldane, 1949) for each node in the ML species-phylogeny, determining the relative change from the root node (putative extratropical ancestor) to each node. This allowed us to evaluate whether ancestral values at basal nodes were retained throughout the tree. We called this statistic *droot.* We used absolute values of *droot* to prevent opposing changes from averaging out to zero, ensuring that mean estimates reflect the magnitude of evolutionary change regardless of direction. Unlike standard phylogenetic signal metrics (e.g., Pagel’s lambda and Bloomberg’s K), which assess trait similarity due to shared ancestry, *droot* measures the magnitude of change in reconstructed latitude from the root to each node, making it more appropriate for assessing ancestral trait conservatism across the tree. We employed a likelihood-based framework based on a generalized linear model (GLM) without an intercept assuming a Gaussian distribution with a logarithmic link to account for the right-skewed distribution of absolute *droot* values of all traits together (Figure 4B). Model coefficients estimated the mean absolute *droot* for each trait and were tested against the overall mean absolute *droot* as a proxy for the basal rate of change using Wald's tests (and package's wald.test function; Lesnoff & Lancelot, 2012). To control false discovery rates, *p*-values were adjusted using the Benjamini-Hochberg's (BH) method (R's *p.adjust* function; Benjamini & Hochberg, 1995), with a significance threshold of 0.01 to minimize Type I errors. Traits with mean *droot* values lower than or equal to the background rate were considered to show ancestral trait conservatism across the phylogeny. Additionally, pairwise t-tests with BH-adjusted *p*-values were conducted in R to compare absolute *droot* means across traits. Finally, for each trait we performed a simple linear regression to evaluate if *droot* varied across phylogenetic scales (*droot* ~ *node_depth*) using wald-tests on slope parameters; slope values ≈ 0 suggest no shifts in *droot* across phylogenetic scales whereas positive values would suggest higher changes in deeper nodes. A detailed explanation of these methods can be found in the Supplementary Methods.

3. Results

3.1. Specimen-level phylogeny. After identification and removal of putative hybrids, we obtained a dataset of 234 accessions for the specimen-level phylogeny (Fig. 1A, Supplementary Fig. 1, Appendix 2). The concatenated alignment was 27,072 bp in length (752 loci) and contained 31.91% missing data. In the ML phylogeny, all accessions of a given species formed monophyletic groups except for

Weinmannia reticulata Ruiz & Pav. Two different subclades, named *W. reticulata1* and *W. reticulata2*, were treated as separate species for the purpose of the present analysis (Supplementary Fig. 1). Our analysis also included accessions of undetermined species (sp1–7) that showed morphological and phylogenetic cohesion. Overall, the specimen-level phylogeny showed a strong geographic structure within South American *Weinmannia*, with clades each containing specimens collected in the same region. Species from the Northern Andes (Ecuador and Colombia) formed a clade nested within the *Weinmannia* crown group that included the species sampled from the Central Andes (Bolivia and Peru), Southern Andes (Chile) and Reunion Island (Fig. 1A, Supplementary Figs. 1,2).

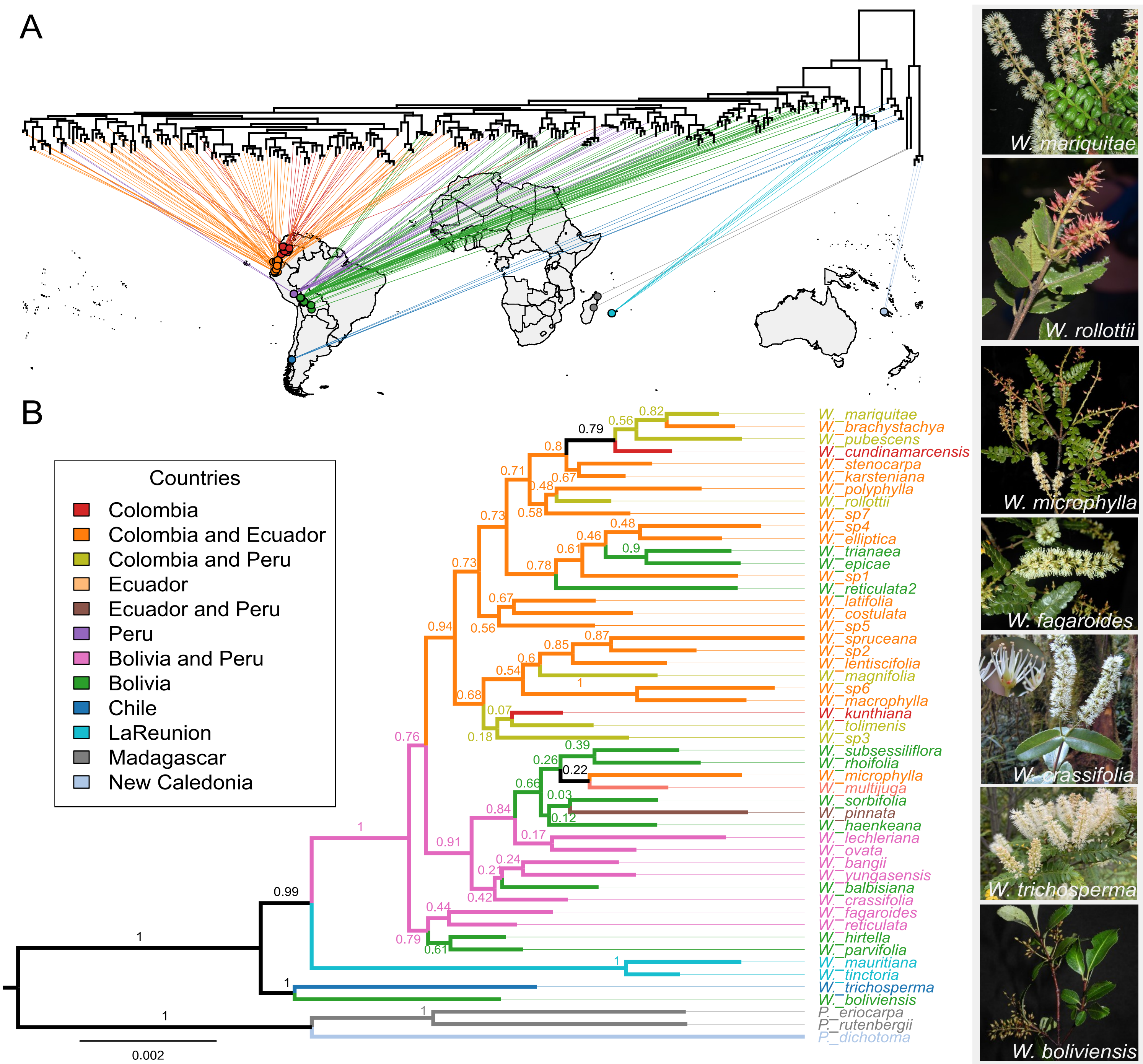

Figure 1. Geographic structure of phylogenetic (ML tree) relationships in *Weinmannia*. A. Specimen-level phylogeny with tips projected onto geographic locations. B. Species-level phylogeny for *Weinmannia*. Bootstrap support values are shown as node labels. Tip labels and branches are colored by the country where species were collected. Field pictures: *W. mariquitae*, *W. rollottii*, (photo credit: Francisco Fajardo); *W. microphylla*, *W. fagaroides* and *W. crassifolia* (Photo credit: William Farfan-Rios); *W. trichosperma* (photo credit: Diego Penneckamp); and *W. boliviensis* (photo credit: Alfredo Fuentes).

3.2. Species-level phylogeny

The character matrix for the species-tree reconstruction contained 103,676 bp (2,879 loci), with 48.63% missing data, for 51 taxa. The concatenated ML species tree (ML; Fig. 1B) and the multi-species coalescent model-based species tree (hereafter SVDQ tree; Supplementary Fig. 3) both showed strong bootstrap support [Bootstrap Support (BS) = 1 in both cases] for genus *Weinmannia*, confirming its monophyly. The time-calibrated phylogeny based on the ML topology showed that the MRCA of *Weinmannia* diverged from the outgroup in the late Eocene around 34.4 Ma and started to diversify ~20.7 Ma (Fig. 2), with similar results observed in the SVDQ tree analysis (~21.38 Ma; Supplementary Fig. 4). Congruent with our specimen-level phylogeny, the species-level phylogenies also showed a general trend where geographically proximate taxa were found in the same clade (Fig. 1B; Supplementary Figs. 1 and 2).

In the ML species tree, *Weinmannia trichosperma*, the southernmost species located in the temperate, extratropical forests of southern South America, was placed in a clade that was strongly supported as the sister group to the remaining species of *Weinmannia* (BS = 1; Fig. 1B), along with *Weinmannia boliviensis* R.E.Fr., the southernmost species in the central Andes inhabiting the subtropical Tucuman-Bolivian forests. The ML phylogeny also shows that *W. trichosperma* and *W. boliviensis* diverged from each other 17.9 Ma, which is older than the onset of diversification in the tropical Andean clade, which is dated at 13.8 Ma (Fig. 2). In contrast, our SVDQ tree shows a topology with *W. boliviensis*, a clade consisting of the two Mascarene species, and then *W. trichosperma* as successive sister groups to the remaining *Weinmannia* species (supplementary Figs. 2 and 3). Despite the topological differences between these two trees, both strongly support the placement of the southernmost lineages *W. trichosperma* and *W.*

boliviensis, alongside *W. mauritiana* and *W. tinctoria*, as sister lineages to the remainder of *Weinmannia* in the phylogeny, supporting our original prediction regarding the southern origin of American *Weinmannia*.

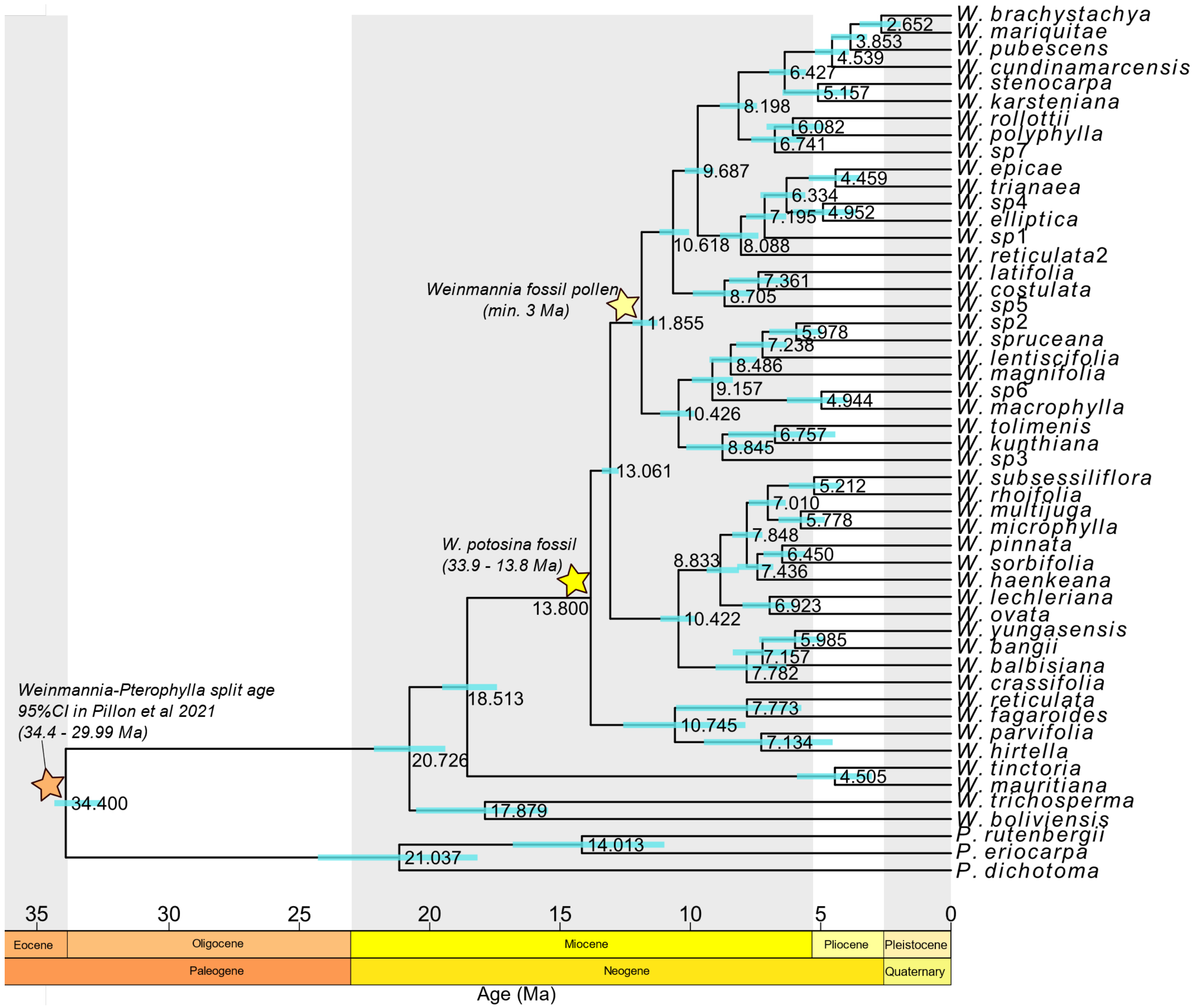

Figure 2. Maximum likelihood phylogeny with estimated divergence times of *Weinmannia* species. Median divergence age estimates across bootstrap trees with 95% confidence intervals in blue bars. Time calibration nodes are indicated with stars.

3.3. The tropical Andean clade shows geographic structure in the Central and Northern Andes. Following the divergence of *Weinmannia* in southern South America and the Mascarenes, the remaining 44 species, which are found exclusively in the tropical Andes, formed a large, strongly supported clade (BS=1 in Fig. 1B for ML; and BS= 0.98 in Supplementary Fig. 2 for SVDQ), which started to diversify ~13.8 Mya (Fig. 2 and Supplementary Fig. 4). Even accounting for the topological differences between the SVDQ and ML trees (Supplementary Fig. 3), the Tropical Andean clade exhibited clear geographic structure. The ML reconstruction shows two clades at its base, the first containing four species from Bolivia and Peru (BS= 0.79; Fig. 1B), and its sister clade (BS=0.76; Fig. 1B), which bifurcated into two major clades. The first of these clades was strongly supported (BS=0.91; Fig. 1B) and included 13 species from the central Andes, with exceptions such as *Weinmannia multijuga* Killip & A.C.Sm. from Peru and Colombia, *Weinmannia pinnata* L. from Peru and Ecuador, and *Weinmannia microphylla* Ruiz & Pav. from Ecuador. The second of these clades was also well supported (BS = 0.84; Fig. 1B) and included most species from the northern Andes (Ecuador and Colombia), except for *Weinmannia trianae* Wedd., *Weinmannia epicae* A. Fuentes, and what we call *Weinmannia reticulata2* from Bolivia (Fig. 1B).

Our SVDQuartets species tree showed a similar pattern for the Tropical Andes clade, in that it was divided into two major clades. The first contained 16 species, all found in the central Andes of Bolivia and Peru, except for *W. multijuga*, which is found from Colombia to Peru (BS= 0.83, Supplementary Fig. 2). The second clade was well supported (BS=0.84) and contained the remaining 28 species, all from the northern Andes except *W. reticulata2* and *W. balbisiana* Kunth from Bolivia (Supplementary Fig. 2).

3.4. Younger clades are distributed towards northern latitudes. Ancestral state reconstructions for latitudes in internal nodes of the phylogeny for American species show that nodes with older divergence times are more likely to be associated with more southern reconstructed latitudes. Likewise, nodes with younger divergence times are more likely to be associated with more northern reconstructed latitudes (Figs. 3A and 3B, and Supplementary Fig. 5A). This also supports our initial prediction, indicating a northward progression in the diversification of *Weinmannia* in the Andes.

Our Bayesian model predicting node age as a function of reconstructed latitude on the ML phylogeny yielded a maximum *a posteriori* (MAP) slope for latitude (β) of -0.486. The 99% credible interval estimated for this parameter ranged from -0.795 to -0.201, which does not include zero, providing robust evidence to reject the null hypothesis (β=0; Fig. 3C) of no relationship between node age and latitude. Using our SVDQ topology with ML-optimized branch lengths we observed identical results, where nodes with shorter distance from the root tended to be associated with more southern latitudes (MAP for slope = -0.337) with the null hypothesis rejected with a 99% credible interval ranging from -0.555 to -0.0975 (Supplementary Fig. 5C). Accordingly, the results of the NHST with nonparametric bootstrap on the slope coefficient also showed that node age tended to be negatively related to ancestral latitude when using both our ML tree topology (slope = -0.481±0.101; p-value = 0.00000, Supplementary Fig. 6A) and SVDQ topology (slope= -0.315±0.074; p-value =0.00002, Supplementary Fig 6B). Likewise, we obtained equivalent results for both ML and SVDQ topologies and statistical methods when we included the two Mascarene species in the analysis (Supplementary Figs. 6C,6D and Supplementary Figs. 7,8).

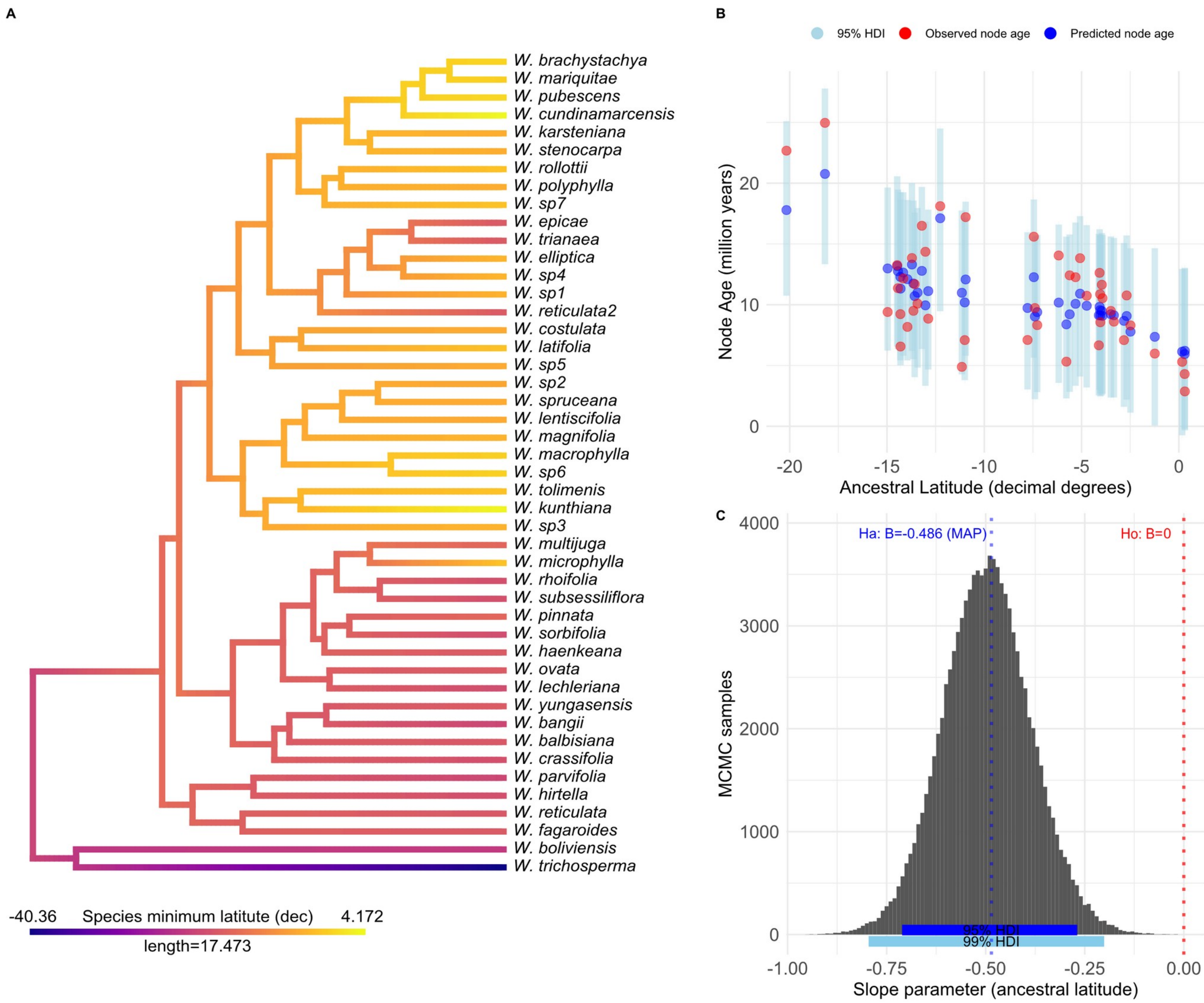

Figure 3. Analyses of migration from southern latitudes to the northern Andes using the ML topology, excluding Mascarene species. A. Ancestral character reconstruction for latitude of hypothetical ancestors (nodes). The colors depict a continuous gradient of latitude, transitioning from southern temperate regions in blue to northern tropical regions in yellow, with intermediate latitudes in the central Andes represented in red. B. Bayesian linear regression of node age as a function of predicted ancestral latitude. Observed values are represented in red dots. The blue dots represent the maximum *a posteriori* estimates and the sky blue bars represent 95% High Density Intervals (HDI) of model-predicted node ages. C. *A posteriori* probability distribution for the estimated slope coefficient for latitude as a predictor of node age with 95% and 99% HDI indicated with blue and skyblue bars.

3.5. Despite variation in elevation and latitude, the extratropical climatic niche remained stable. Results of ancestral character reconstruction (Supplementary Fig. 9) showed that all climatic variables with the exception of Temperature Seasonality

(BIO4) and Precipitation of the Coldest Quarter (BIO19) tended to show little change across the phylogeny, with values generally remaining similar to those found in the MRCA of the *trichosperma-boliviensis* clade (Supplementary Figs. 10 A to S). Moreover, the mean absolute *droot* estimates for conserved climatic variables were statistically lower or equal to the background *droot* (Figs. 4A and 4B, Supplementary Table 1). In contrast, reconstructed ancestral Latitude, Elevation, Temperature Seasonality (BIO4) and Precipitation of the Coldest Quarter (BIO19; winter rain) showed greater changes over evolutionary time, all showing absolute *droot* values that were statistically different and higher than the background *droot* (Fig. 4A, Supplementary Table 1). These results indicated that species shifted away from the MRCA of the extant extratropical lineage (containing *trichosperma-boliviensis)* towards higher elevations and equatorial (closer to zero) latitudes over evolutionary time. Accordingly, the non-conserved variables BIO4 and BIO19 are expected to vary along the latitudinal gradient, aligning with expected reduced temperature seasonality and less predictable winter rainfall closer to the equator. A likelihood ratio test against the null model assuming no differences between the rates of change of variables (deviance=0.153, df1=965, df=945, *p*-value = 2.2e-16) and paired t-test comparisons for absolute *droot* means between all pairs of variables (Fig. 4C) showed statistically significant differences in *droot* between all 19 reconstructed climatic variables and both elevation and latitude, with the exception of BIO19 and BIO14. Values lower and equal to the background rates of change for most climatic variables suggest conservatism of the climatic niche as the lineages dispersed towards more equatorial latitudes and higher elevations. Further, regression analysis of the *droot* metric as a function of node depth also supports the notion of climatic niche stability across phylogenetic scales for BIO1 (slope=0.00001, *p*-value =0.95), BIO12 (slope=0.00013, *p*-value =0.32), and all other climatic variables (Supplementary Fig. 10A to S), as opposed to elevation (slope = 0.00043, *p*-value < 0.05) and latitude (slope = 0.00048, *p*-value < 0.05), which both displayed positive slopes significantly different than zero, reflecting more evolutionary changes at deeper nodes (Supplementary Figs. 10T and U).

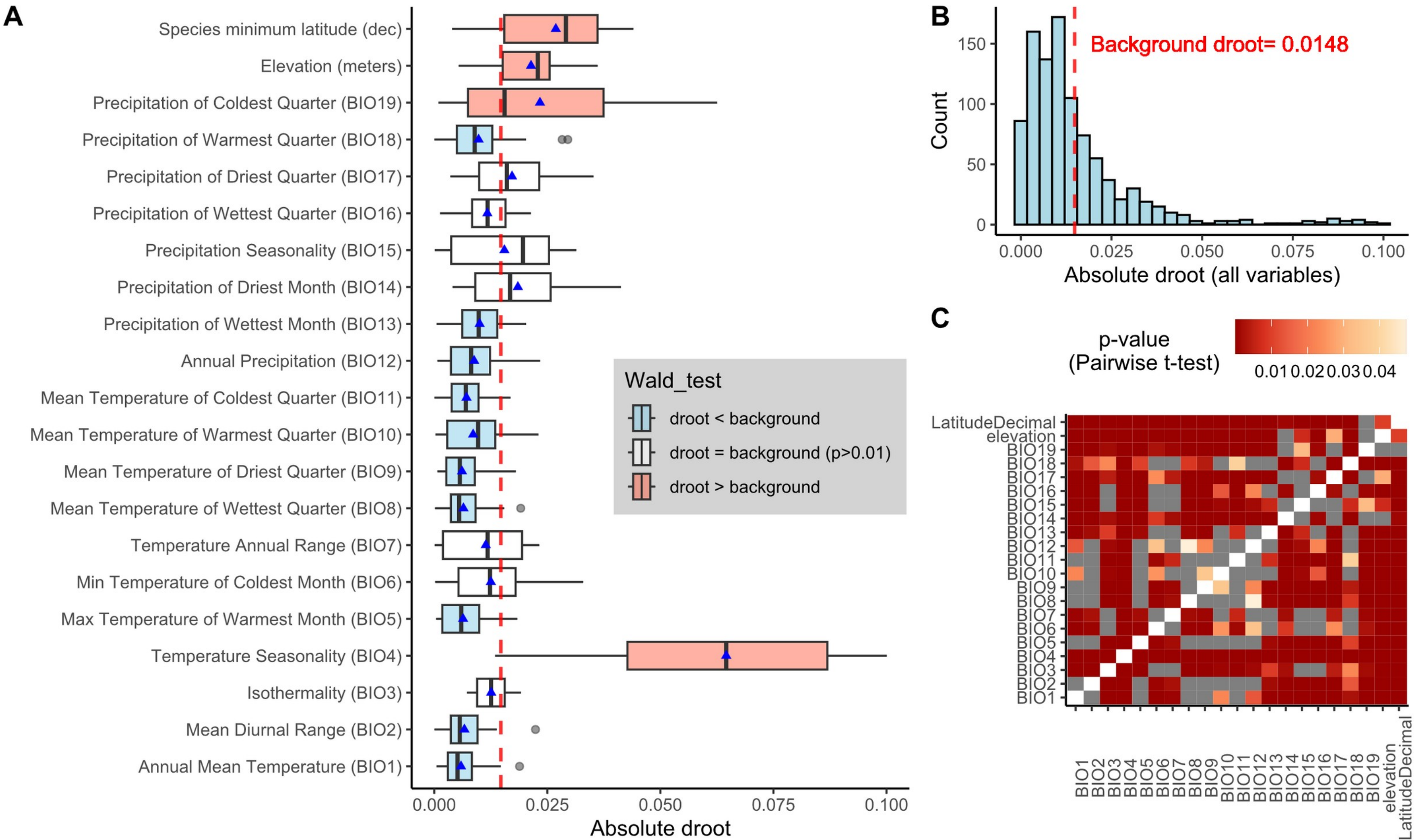

Figure 4. Comparison of evolutionary rates (absolute *droot*) from each node to the MRCA of *Weinmannia*. A. Boxplots show absolute *droot* values for ancestral reconstructions of 19 climatic variables (BIO1-BIO19), elevation, and latitude. Dashed red line shows the background (mean) *droot* across all variables. White boxplots indicate variables with *droot* values not statistically different from the background rate ($p > 0.01$). Light blue and red boxplots indicate variables with *droot* values lower and higher than the background rate ($p < 0.01$) *droot* based on a Wald test. Blue triangles represent the mean *droot* for each variable. B. Histogram showing right-skewed distribution of absolute *droot* values across all variables. C. Heatmap showing BH adjusted *p*-values of pairwise t-test comparisons between *droot* means of variables. Pairs with a *p*-value>0.05 are shown in grey.

4. Discussion

Our analyses of *Weinmannia* reveal that extratropical species are placed as the basally branching lineages in the phylogeny. We also found a robust negative relationship between the age of clades and their latitudinal distribution across the phylogeny, suggesting a south-to-north dispersal route. In addition, we show that *Weinmannia* exhibits strong environmental niche conservatism despite showing large changes in elevation and latitude. These results align with fossil evidence that has sparked the hypothesis that *Weinmannia* may have originated from a lineage that was pre-adapted to the climatic conditions of the southern extratropics, and that the arrival and diversification of *Weinmannia* in the American tropics occurred when suitable climates were created as a result of the Andean uplift.

4.1. An extratropical origin for *Weinmannia*

Our ML phylogeny places *Weinmannia trichosperma* from the temperate forests of southern South America in a clade that is sister to all other species of *Weinmannia* (ML, BS = 1, Fig. 1). This is consistent with previous morphological and genetic reconstructions of the phylogenetic relationships of species in the genus (Bradford, 1998, 2002), but is slightly different from results with our SVDQ approach (Supplementary Fig. 2). Also consistently placed among the oldest diverging lineages is the subtropical species *Weinmannia boliviensis* (Fig. 1a and S2). *W. boliviensis* is distributed in the Tucuman-Bolivian forests (Harling and Fuentes, 2014), which are subtropical montane forests on the eastern slope of the Andes, extending from 23°S to 29°S (Cabrera, 1976). According to our ML phylogeny, *W. boliviensis* and *W. trichosperma* diverged during the Miocene (~17.9 Ma. Fig. 2), older than the ancestral node for the tropical species (~13.8 Ma. Fig. 2).

Furthermore, this date precedes the final uplift of the central and southern Andes to their present elevations (above 3000 m), which began during the late Miocene (~11 Ma) (Gregory-Wodzicki, 2000; Siravo et al., 2018), and the subsequent expansion of arid areas to the west and east of the mountain range (Rambo, 1952; Palazzesi et al., 2014). Therefore, the evolutionary divergence at the base of *Weinmannia* would have occurred in forests composed of Gondwanan lineages that persisted in the southern extratropics during the Paleogene and Neogene (Romero, 1986), which were deeply isolated from the tropical lowland flora by environmental rather than geographic factors (Jaramillo and Cárdenas, 2013) and accumulated their own evolutionary uniqueness (Segovia et al., 2020).

The phylogenetic results presented here are consistent with fossil evidence suggesting that the family Cunoniaceae originated and rapidly diversified in Gondwana during the Cretaceous, and that *Weinmannia* and its sister lineages had a widespread distribution across the southern extratropics during the Paleogene. The early diversification of Cunoniaceae is well known from macrofossils from the Cretaceous to Paleogene of Antarctica (Poole et al., 2000, 2001, 2003) and the Cenozoic of both Australia (Barnes, 1999; Barnes and Hill, 1999; Barnes and Jordan, 2000; Barnes et al., 2001) and southern South America (Gandolfo and Hermsen, 2017; Jud et al., 2018; Jud and Gandolfo, 2021). A few putative Cretaceous fossils of Cunoniaceae have also been collected from Laurasian deposits in Europe (Schönenberger et al., 2001) and North America (Tang et al., 2020), as well as from Myanmar in the northern hemisphere (Poinar and Chambers, 2017). Although these fossils would deviate from the established high-latitude, southern hemisphere origin and diversification of Cunoniaceae, their taxonomic affinities still remain uncertain, requiring future research involving detailed morphological and phylogenetic characterization (Carpenter and Rozefelds, 2021, but see Tang et al., 2022). In any case, fossil evidence also suggests that Cunoniaceae family would have been more diverse during the Upper Cretaceous and Paleogene in Patagonia and Antarctica than it is today, as most fossils have not been placed in any extant genus (Jud and Gandolfo, 2021; Matel et al., 2021). Furthermore, paleontological records demonstrate that the Cunoniaceae family was widespread across Gondwana during the Paleocene, a period when warm climates fostered floristic exchange between South America and Australia through Antarctica (Hallam, 1995; Sanmartín and Ronquist, 2004; Cantrill and Poole, 2012; Wilf et al., 2013). Similarly, ancestors of the *Weinmannia* lineage would have had a wider distribution during the Paleogene, when the climate in Patagonia was warmer and wetter than today, and Australia was further south (Jud and Gandolfo, 2021). Indeed, an early Oligocene (~30 Ma) macrofossil record, *Weinmanniaphyllum bernardii* R.J. Carp. & A.M. Buchan from extratropical Tasmania (Carpenter and Buchanan, 1993; Carpenter and Rozefelds, 2021), where the genus is now extinct, is morphologically similar to *W. trichosperma* from temperate forest in Southern South America (Bradford, 1998).

The limited number of *Weinmannia* species in the modern extratropics (subtropical and temperate forests), particularly as compared to their diversity in the tropical Andes is likely a result of later extinction processes at higher latitudes. The extinction of *Weinmannia* outside of its modern range in the Americas and the Mascarenes may be related to a sharp reduction in forest cover due to the formation of the Antarctic Ice Sheet in the early Oligocene, which was associated with a massive extinction of the Austral paleoflora across the southern hemisphere (Francis, 1996; Truswell and Macphail, 2009). A subsequent extinction event, triggered by increased aridity due to the Andean orogeny and other influences (Palazzesi et al., 2014), likely resulted in a northward expansion of *Weinmannia* in South America, with surviving populations restricted to the Pacific coast of southern

South America, the Brazilian plateau and the tropical slopes of the Andes (Jud and Gandolfo, 2021).

4.2. South-to-North dispersal and climatic niche conservatism through the Andean Corridor

The robust negative relationship between node age and latitude in our phylogeny reveals a late arrival of the lineage in the tropics and a south-to-north dispersal route along the Andes (Fig. 3 and Supplementary Figs. 5 and 6). This scenario is consistent with fossil evidence showing that the oldest pollen records of *Weinmannia* in the northern Andes are from the late Pliocene and Pleistocene (1.5–3.2 Ma) (Van der Hammen et al., 1973). The crown age of the Northern Andes clade recovered in the present study is estimated at 11.9 Ma (Fig. 2), predating the earliest fossil evidence for *Weinmannia* in the region by several million years. However, this estimate aligns with the time frame in which suitable habitats are thought to have become available (Luebert and Weigend, 2014). Thus, this inconsistency may be due to the low preservation potential of the pollen or sampling intensity in the fossil record, which can cause the date of the first fossil appearance to be significantly younger than the true arrival date of a taxon in a region (Smith and Peterson, 2002).

The phylogenies generated in this study have provided strong evidence for the direction of the dispersal of *Weinmannia*, even though tree topologies differed somewhat between RAxML and SVDQuartets. These differences in phylogenetic tree topologies when using SVDquartets and RAxML (Supplementary Fig. 3) may be due to their different underlying principles and methodologies. SVDquartets uses a quartet-based approach that relies on gene coalescence patterns without imposing specific evolutionary models, allowing it to account for complex evolutionary signals such as incomplete lineage sorting or hybridization. In contrast, RAxML is a maximum likelihood-based method that operates under defined evolutionary models to estimate relationships and branch lengths, potentially yielding a simpler tree structure. Despite the differences in methods, the overarching patterns remain robust across phylogenetic reconstruction approaches, with both SVDquartets and RAxML revealing similar geographic structures. Both methods consistently identified a clade containing nearly all species from the northern Andes nested within a broader clade containing all species from the central and southern Andes (Fig. 1 and Supplementary Fig. 2). Although the trees show slight differences in statistical support, the robust trend of northern lineages appearing more recently suggests that lineage dispersal likely followed a northward progression through the Andes (Fig. 3 and Supplementary Figs. 5 and 6).

Given the south-to-north dispersal route, the high climatic niche conservatism found in *Weinmannia* (Fig. 4, Supplementary Figs. 9 and 10 and Supplementary Table 1) suggests that the lineage first evolved under the environmental conditions of the southern extratropics and maintained these adaptations during south-to-north dispersal. Our results show that the MRCA of *Weinmannia* likely occupied a niche with relatively cool mean annual temperatures (~14.63°C) and mid-to-high mean annual precipitation (~1294.7mm; Supplementary Fig. 10). This extratropical niche has remained stable throughout the evolutionary history of the clade, with ancestral mean annual temperature and precipitation (BIO1 and BIO12), among almost all other climatic variables, showing little change across the phylogeny (Fig. 4 and Supplementary Fig. 10). In contrast, the larger changes observed in Latitude, Elevation, Temperature Seasonality (BIO4) and Winter Precipitation (BIO19) reflect the dynamic nature of *Weinmannia's* elevational shifts, as lineages moved to more equatorial latitudes over evolutionary time (Fig. 4 and

Supplementary Figs. 9 and 10). Plant lineages often exhibit a high degree of phylogenetic niche conservatism (Crisp et al., 2009), and this tendency to maintain a stable climatic niche likely allowed *Weinmannia* and other extratropical lineages to rapidly colonize similar environments created at mid- and high- elevations following the uplift of the Andes at equatorial latitudes (Donoghue, 2008; Segovia and Armesto, 2015). This is consistent with the notion that pre-adapted clades like *Weinmannia* followed their temperature and precipitation preferences during dispersal, while simultaneously adjusting to the varied elevations encountered in tropical mountain ecosystems. These results support the idea that ecological sorting of pre-adapted clades had a significant influence in shaping Andean tree communities (Ramírez et al., 2019; Griffiths et al., 2020; Linan et al., 2021a).

4.3. The intriguing history of the Mascarenes' *Weinmannia*

Both our ML and SVDQ phylogenies show that a small clade containing two species from the western Indian Ocean, *Weinmannia tinctoria* Sm. and *Weinmannia mauritania* D.Don, is nested within South American *Weinmannia* (Fig. 1 and Supplementary Fig. 2), which confirms previous phylogenetic reconstructions (Bradford, 2002). This result is surprising because it implies a long-distance dispersal event, but with the stem age (~18.513 Ma, Fig. 2 and ~ 19.749 Ma, Supplementary Fig. 4) of the Mascarene clade older than the volcanic origin of the archipelago (less than 8 Ma, McDougall and Chamalaun, 1969). Furthermore, this result is unexpected because botanical affinities and phylogenetic evidence suggest that Madagascar may have acted as a source of diversity for the Mascarenes (Linan et al., 2019), but no species of *Weinmannia* are currently found in Madagascar or Africa (Pillon et al., 2021). Thus, any model for the dispersal of *Weinmannia* from

South America should likely involve Madagascar or Africa as a cryptic stepping-stone to reach the Mascarenes. In any case, further studies are needed to properly address this intriguing disjunction and to clarify possible vicariant or long-distance dispersal events in the origin of the genus *Weinmannia*.

5. Conclusion

Weinmannia reflects a pattern in which a lineage of extratropical origin shows lower species richness in the extratropics than in the recently colonized tropics. This pattern has also been proposed for the entire family Cunoniaceae (Pillon et al., 2021), which has traditionally been considered a lineage derived from the "Gondwanan" center of plant diversification (Raven and Axelrod, 1974). Furthermore, the fossil record indicates that the Cunoniaceae family was present in Antarctica (i.e., western Gondwana) during the Late Cretaceous (~70 Ma), along with a highly diverse vegetation similar in taxonomic composition to the temperate forests of southern South America today (Poole et al., 2003). This suggests that the biogeographic history of *Weinmannia* and Cunoniaceae may have been shared with other lineages from the so-called Austral Floristic Realm, which likely served as a source of biodiversity contributing to the hyperdiversity of plants in the Andes.

6. Availability of data and codes

All raw sequence data used in this study are deposited in the NCBI SRA database (BioProject accession number PRJNA1237785). The alignments, trees and codes can be found at the Dryad Digital Repository: https://datadryad.org/stash/share/oByZiKhEUtrkZSA0il4UZ87iem2Gr72GKBScMfX08TU

7. Acknowledgements

The study was supported by FONDECYT 11200967 and the National Science Foundation (DEB 1836353). R.A.S is supported by Institute of Ecology and Biodiversity (IEB) ANID grant FB210006, F.F.G. was supported by the Shirley A. Graham Fellowships 2022 in Systematic Botany and Biogeography of the Missouri Botanical Garden. C.E.E. and the Conservation Genetics Program at the Missouri Botanical Garden is supported by donations from Stephen and Camilla Brauer, Philip and Sima Needleman, and the Bellwether Foundation. Collections in Ecuador were partially funded by Universidad Tecnológica Indoamérica, NHO. We thank the Ministerio del Ambiente, Agua y Transición Ecológica in Ecuador for collecting permits (contrato marco MAE-DNB-CM-2019-011).

References

Achá S., Linan A., MacDougal J., Edwards C. 2021. The evolutionary history of vines in a neotropical biodiversity hotspot: Phylogenomics and biogeography of a large passion flower clade (*Passiflora* section *Decaloba*). *Mol. Phylogenetics Evol*. 164:107260.

Antonelli A., Sanmartín I. 2011. Why are there so many plant species in the Neotropics? *Taxon* 60:403–414.

Antonelli A., Zizka A., Silvestro D., Scharn R., Cascales-Miñana B., Bacon C. D. 2015. An engine for global plant diversity: highest evolutionary turnover and emigration in the American tropics. *Frontiers in Genetics* 6:130.

Bacon C.D., Velásquez-Puentes F.J., Hinojosa L.F., Schwartz T., Oxelman B., Pfeil B., Arroyo M.T.K., Wanntorp L., Antonelli A. 2018. Evolutionary persistence in *Gunnera* and the contribution of southern plant groups to the tropical Andes biodiversity hotspot. *PeerJ* 6: e4388.

Balslev H. 1993. Introduction. In: Balslev H., editor, *Neotropical Montane Forests – Biodiversity and Conservation*. Aarhus, Denmark: AUU Reports 31, Aarhus University Press.

Barnes R.W., Hill R.S. 1999. *Ceratopetalum* fruits from Australian Cainozoic sediments and their significance for petal evolution in the genus. *Australian Systematic Botany* 12:635–645.

Barnes R.W., Jordan G.J. 2000. *Eucryphia* (Cunoniaceae) reproductive and leaf macrofossils from Australian Cainozoic sediments. *Australian Systematic Botany* 13:373–394.

Barnes R.W., Hill R.S., Bradford J.C. 2001. The history of Cunoniaceae in Australia from macrofossil evidence. *Australian Journal of Botany* 49:301–320.

Benjamini, Y., and Hochberg, Y. 1995. Controlling the false discovery rate: a practical and powerful approach to multiple testing. *Journal of the Royal Statistical Society Series B*, 57, 289–300.

Berry E.W. 1917. The Age of the Bolivian Andes. *Proc. Natl. Acad. Sci. U.S.A.* 3:283–285.

Bradford J.C. 1998. A cladistic analysis of species groups in *Weinmannia* (Cunoniaceae) based on morphology and inflorescence architecture. *Ann. Missouri Bot. Gard.* 85:565-593.

Bradford J.C. 2002. Molecular phylogenetics and morphological evolution in Cunonieae (Cunoniaceae). *Ann. Missouri Bot. Gard.* 89:491-503.

Bradford J. C., Fortune-Hopkins H. C. Barnes R. W. 2004 *Cunoniaceae*. In The families and genera of vascular plants (ed. K. Kubitzki), pp. 91–111. Heidelberg, Germany: Springer.

Cabrera A.L. 1976. Regiones fitogeográficas argentinas. *Enciclopedia Argentina de Agricultura y Jardinería* 2:1-85.

Cantrill D.J., Poole I. 2012. The vegetation of Antarctica through geological time. Cambridge: Cambridge University Press.

Carpenter B., Gelman A., Hoffman M.D., Lee D., Goodrich B., Betancourt M., Brubaker M., Guo J., Li P., Riddell A. 2017. Stan: A Probabilistic Programming Language. *J. Stat. Soft*. 76:1–32.

Carpenter R.J., Buchanan A.M. 1993. Oligocene leaves, fruit and flowers of the Cunoniaceae from Cethana, Tasmania. *Aust. Syst. Bot.* 6:91-109.

Carpenter R.J., Rozefelds A.C. 2021. Gondwanan or global? A commentary on: "Fossil evidence from South America for the diversification of Cunoniaceae by the earliest Palaeocene." *Annals of Botany* 127(3):iii–v.

Chacón, J., de Assis, M. C., Meerow, A. W., Renner, S. S. 2012. From east Gondwana to Central America: historical biogeography of the Alstroemeriaceae. *Journal of Biogeography:* 39(10), 1806-1818.

Chifman J., Kubatko L. 2014. Quartet Inference from SNP Data Under the Coalescent Model. *Bioinformatics:* 30:3317–3324.

Crisp M. D., Arroyo M. T., Cook L. G., Gandolfo M. A., Jordan G. J., McGlone M. S., Weston P.H., Westoby M., Wilf P., et al. 2009. Phylogenetic biome conservatism on a global scale. *Nature* 458: 754-756.

Donoghue M.J. 2008. A phylogenetic perspective on the distribution of plant diversity. *Proc. Natl. Acad. Sci.* 105:11549-11555.

Doyle J.J., Doyle J.L. 1987. A rapid DNA isolation procedure for small quantities of fresh leaf tissue. *Phytochem. Bull*. 19:11–15.

Drummond A. J. Rambaut A.2007. BEAST: Bayesian evolutionary analysis by sampling trees. *BMC Evol. Biol.* 7:214.

Earl D.A., von Holdt B.M. 2012. STRUCTURE HARVESTER: a website and program for visualizing STRUCTURE output and implementing the Evanno method. *Conserv. Genet. Resour.* 4: 359-361.

Eaton D.A.R., Overcast I. 2020. ipyrad: interactive assembly and analysis of RADseq datasets. *Bioinformatics.* 36:2592–2594.

Fick S.E., Hijmans R.J. 2017. WorldClim 2: new 1-km spatial resolution climate surfaces for global land areas. *International Journal of Climatology* 37, 4302–4315.

Francis J.E. 1996. Antarctic palaeobotany: clues to climate change. *Terra Antarctica* 3:135–140.

Gandolfo M.A., Hermsen E.J. 2017. *Ceratopetalum* (Cunoniaceae) fruits of Australasian affinity from the early Eocene Laguna del Hunco flora, Patagonia, Argentina. *Annals of Botany* 119:507–516.

González-Caro S., Tello J.S., Myers J.A., Feeley K., Blundo C., Calderón-Loor M., Carilla J., Cayola L., Cuesta F., Farfán W., et al. 2023. Historical Assembly of Andean Tree Communities. *Plants* 12:3546.

Graham, A. 1973. History of the arborescent temperate element in the northern Latin American biota. Vegetation and vegetational history of northern Latin America, 301-314.

Graham, A. 1995. Development of affinities between Mexican/Central American and northern South American lowland and lower montane vegetation during the Tertiary. Pp. 11-22 in S. P. Churchill, H. Balslev, E. Forero & J. L. Luteyn (editors), Biodiversity and Conservation of Neotropical Montane Forests. New York Botanical Garden, Bronx.

Graham A., Gregory-Wodzicki K.M., Wright K.L. 2001. Studies in Neotropical Paleobotany. XV. A Mio-Pliocene palynoflora from the Eastern Cordillera, Bolivia: implications for the uplift history of the Central Andes. *American Journal of Botany* 88, 1545–1557.

Gregory-Wodzicki K.M. 2000. Uplift history of the Central and Northern Andes: a review. *Geol. Soc. Am. Bull.* 112:1091-1105.

Griffiths A.R., Silman M.R., Farfán Rios W., Feeley K.J., García Cabrera K., Meir P., Salinas N., Dexter K.G. 2020. Evolutionary heritage shapes tree distributions along an Amazon-to-Andes elevation gradient. *Biotropica* 53:38–50.

Griffiths, A.R., Silman, M.R., Farfan-Rios, W., Feeley, K.J., Cabrera, K.G., Meir, P., Salinas, N., Segovia, R.A., Dexter, K.G. 2021. Evolutionary diversity peaks at mid-elevations along an Amazon-to-Andes elevation gradient. *Frontiers in ecology and evolution*, 9, 680041.

Haldane J.B.S. 1949. Suggestions as to Quantitative Measurement of Rates of Evolution. *Evolution* 3, 51–56.

Hallam A. 1995. An outline of Phanerozoic biogeography. Oxford: Oxford University Press, 256 pp.

Harling G.W. Fuentes A.F. 2014. Cunoniaceae. In: P.M. Jørgensen, M.H. Nee, S.G. Beck, editors. *Cat. Pl. Vasc. Bolivia, Monogr. Syst. Bot. Missouri Bot. Gard. 127*. St. Louis.USA. Missouri Botanical Garden Press:540–542.

Hooghiemstra H. 1984. Vegetational and climatic history of the high plain of Bogotá, Colombia: A continuous record of the last 3.5 million years. *Diss. Bot.* 79:368.

Hughes, C., & Eastwood, R. 2006. Island radiation on a continental scale: exceptional rates of plant diversification after uplift of the Andes. *Proceedings of the National Academy of Sciences:* 103(27), 10334-10339.

Inglis P.W., Pappas M., Resende L.V., Grattapaglia D. 2018. Fast and inexpensive protocols for consistent extraction of high quality DNA and RNA from challenging plant and fungal samples for high-throughput SNP genotyping and sequencing applications. *PLoS ONE* 13: e0206085.

Jaramillo C., Cárdenas A. 2013. Global warming and neotropical rainforests: a historical perspective. *Annu. Rev. Earth Pl. Sc.* 41:741–766.

Jud N.A., Gandolfo M.A., Iglesias A., Wilf P. 2018. Fossil flowers from the early Palaeocene of Patagonia, Argentina, with affinity to Schizomerieae (Cunoniaceae). *Annals of Botany* 121:431–442.

Jud N.A., Gandolfo M.A. 2021. Fossil evidence from South America for the diversification of Cunoniaceae by the earliest Palaeocene. *Annals of Botany* 127(3):305–315.

Lemoine F., Domelevo Entfellner J.-B., Wilkinson E., Correia D., Dávila Felipe M., De Oliveira T., Gascuel O. 2018. Renewing Felsenstein’s phylogenetic bootstrap in the era of big data. *Nature* 556:452–456.

Lesnoff, M., Lancelot, R. 2012. aod: Analysis of Overdispersed Data. R package version 1.3.3 .http://cran.r-project.org/package=aod

Linan A.G., Schatz G.E., Lowry P.P., Miller A., Edwards C. E. 2019. Ebony and the Mascarenes: the evolutionary relationships and biogeography of *Diospyros* (Ebenaceae) in the western Indian Ocean. *Bot. J. Linn. Soc.* 190: 359-373.

Linan A.G., Myers J.A., Edwards C.E., Zanne A.E., Smith S.A., Arellano G., ... Tello J. S. 2021a. The evolutionary assembly of forest communities along environmental gradients: recent diversification or sorting of pre-adapted clades?. *New Phytol.* 232(6): 2506-2519.

Linan A.G., Lowry II P.P., Miller A.J., Schatz G.E., Sevathian J.-C., Edwards C.E. 2021b. RAD-sequencing reveals patterns of diversification and hybridization, and the accumulation of reproductive isolation in a clade of partially sympatric, tropical island trees. *Molecular Ecology* 30: 4520–4537.

Liu, B., Le, C. T., Barrett, R. L., Nickrent, D. L., Chen, Z., Lu, L.,Vidal-Russell, R. 2018. Historical biogeography of Loranthaceae (Santalales): Diversification agrees with emergence of tropical forests and radiation of songbirds. *Molecular Phylogenetics and Evolution*, 124, 199-212.

Luebert F., Weigend M. 2014. Phylogenetic insights into Andean plant diversification. *Front. Ecol. Evol. 2*:27.

Mashburn B., Jhangeer-Khan R., Bégué A., Tatayah V., Olsen K.M., Edwards C.E. 2023. Genetic assessment improves conservation efforts for the critically endangered oceanic island endemic *Hibiscus liliiflorus*. *J. Hered.* 114:259–270.

Matel T.P., Gandolfo M.A., Hermsen E.J., Wilf P. 2022. Cunoniaceae infructescences from the early Eocene Laguna del Hunco flora, Patagonia, Argentina. *American Journal of Botany* 109(6):986–1003.

Maurin K.J.L. 2008. An empirical guide for producing a dated phylogeny with treePL in a maximum likelihood framework.

McDougall I.A.N., Chamalaun F.H. 1969. Isotopic dating and geomagnetic polarity studies on volcanic rocks from Mauritius, Indian Ocean. *Geol. Soc. Am. Bull.* 80:1419-1442.

Myers N., Mittermeier R., Mittermeier C., da Fonseca G.A.B., Kent J. 2000. Biodiversity hotspots for conservation priorities. *Nature* 403:853–858.

Neves D.M., Dexter K.G., Baker T.R., Coelho de Souza F., Oliveira-Filho A.T., Queiroz, L.P., Lima H.C., Simon M.F., Lewis G.P., Segovia R.A., et al. 2020. Evolutionary diversity in tropical tree communities peaks at intermediate precipitation. *Sci. Rep.* 10:1188.

Owusu S. A., Sullivan A. R., Weber J. R., Hipp A. L. & Gailing, O. 2015. Taxonomic relationships and gene flow in four North American *Quercus* Species (*Quercus* section *Lobatae*). *Systematic Botany*, 40(2), 510–521.

Palazzesi L., Gottschiling M., Barreda V., Weigend M. 2012. First Miocene fossils of Vivianiaceae shed new light on phylogeny, divergence times, and historical biogeography of Geraniales. *Botanical Journal of the Linnean Society* 107:67–85.

Palazzesi L., Barreda V.D., Cuitiño J.I., Guler M.V., Tellería M.C., Santos R.V. 2014. Fossil pollen records indicate that Patagonian desertification was not solely a consequence of Andean uplift. *Nature Communications* 5:3558.

Paradis E., Schliep K. 2019. *ape* 5.0: an environment for modern phylogenetics and evolutionary analyses in R. *Bioinformatics* 35:526–528.

Paris J.R., Stevens J.R., Catchen J.M. 2017. Lost in parameter space: a road map for stacks. *Methods Ecol. Evol.* 8:1360–1373.

Pennington R.T., Dick C.W. 2004. The role of immigrants in the assembly of the South American rainforest tree flora. *Philosophical Transactions of the Royal Society of London. Series B: Biological Sciences* 359:1611-1622.

Pérez-Escobar O.A., Zizka A., Bermúdez M.A., Meseguer A.S., Condamine F.L., Hoorn C., Hooghiemstra H., Pu Y., Bogarín D., Boschman L.M., Pennington R.T., et al. 2022. The Andes through time: evolution and distribution of Andean floras. *Trends Plant Sci.* 27:364-378.

Pillon Y., Hopkins H.C., Maurin O., Epitawalage, N., Bradford, J., Rogers, Z.S., Baker W.J., Forest, F. 2021. Phylogenomics and biogeography of Cunoniaceae (Oxalidales) with complete generic sampling and taxonomic realignments. *Am. J. Bot.* 108:1181-1200.

Poinar G.O. Jr., Chambers K.L. 2017. Tropidogyne pentaptera, sp. nov., a new mid-Cretaceous fossil angiosperm flower in Burmese amber. Palaeodiversity 10:135–140.

Poole I., Cantrill D.J., Hayes P., Francis J. 2000. The fossil record of Cunoniaceae: New evidence from Late Cretaceous wood of Antarctica? *Review of Palaeobotany and Palynology* 111:127–144.

Poole I., Cantrill D.J. 2001. Fossil woods from Williams Point Beds, Livingston Island, Antarctica: a Late Cretaceous southern high-latitude flora. Palaeontology 44:1081–1112.

Poole I., Mennega A.M., Cantrill D.J. 2003. Valdivian ecosystems in the Late Cretaceous and Early Tertiary of Antarctica: further evidence from myrtaceous and eucryphiaceous fossil wood. *Rev. Palaeobot. Palynol.* 124:9-27.

Pritchard J.K., Stephens M., Donnelly P. 2000. Inference of Population Structure Using Multilocus Genotype Data. *Genetics* 155:945–959.

Quiroga M.P., Mathiasen P., Iglesias A., Mill R.R., Premoli A.C. 2016. Molecular and fossil evidence disentangle the biogeographical history of Podocarpus, a key genus in plant geography. *J. Biogeogr*. 43:372-383.

R Core Team. 2023. R: A Language and Environment for Statistical Computing. R Foundation for Statistical Computing, Vienna, Austria. https://www.R-project.org/.

Rahbek C., Borregaard M., Antonelli A., Colwell R., Holt B., Nogués-Bravo D., Rasmussen C., Richardson K., Rosing M., Whittaker R., Fjeldså J. (2019). Building mountain biodiversity: Geological and evolutionary processes. *Science* 365:1114-1119.

Rambo B. 1952. Analise geografica das compostas sul-brasileras. *Sellowia* 5:87–159.

Ramírez S., González-Caro S., Phillips J., Cabrera E., Feeley K.J., Duque Á. 2019. The influence of historical dispersal on the phylogenetic structure of tree communities in the tropical Andes. *Biotropica* 51:500-508.

Raven P.H., Axelrod D.I. 1974. Angiosperm biogeography and past continental movements. *Ann. Missouri Bot. Gard*. 61:539-673.

Revell L.J. 2012. phytools: an R package for phylogenetic comparative biology (and other things). *Methods Ecol. Evol.* 3:217–223.

Revell, L.J., 2024. phytools 2.0: an updated R ecosystem for phylogenetic comparative methods (and other things). *PeerJ* 12, e16505.

Romero E.J. 1986. Paleogene phytogeography and climatology of South America. *Ann. Missouri Bot. Gard*. 73:449–461.

Sanmartín I., Ronquist F. 2004. Southern Hemisphere biogeography inferred by event-based models: plant versus animal patterns. *Systematic Biology* 53:216–243.

Schönenberger J., Friis E.M., Matthews M.L., Endress P.K. 2001. Cunoniaceae in the Cretaceous of Europe: evidence from fossil flowers. *Annals of Botany* 88:423–437.

Segovia R.A., Armesto J.J. 2015. The Gondwanan legacy in South American biogeography. *J. Biogeogr.* 42:209-217.

Segovia R.A., Pennington R.T., Baker T.R., Coelho de Souza F., Neves D.M., Davis C.C., Armesto J.J., Olivera-Filho A.T., Dexter, K. G. 2020. Freezing and water availability structure the evolutionary diversity of trees across the Americas. *Sc. Adv.* 6:eaaz5373.

Siravo G., Fellin M.G., Faccenna C., Bayona G., Lucci F., Molin P., Maden C. 2018. Constraints on the Cenozoic deformation of the northern Eastern Cordillera, Colombia. *Tectonics* 37:4311-4337.

Smith A.B., Peterson K.J. 2002. Dating the time of origin of major clades: molecular clocks and the fossil record. *Annu. Rev. Earth Planet. Sci.* 30: 65-88.

Smith S.A., O'Meara B.C. 2012. treePL: divergence time estimation using penalized likelihood for large phylogenies. *Bioinformatics* 28:2689–2690.

Stamatakis A. 2014. RAxML version 8: a tool for phylogenetic analysis and post-analysis of large phylogenies. *Bioinformatics* 30:1312–1313.

Stan Development Team. 2023. RStan: the R interface to Stan. R package version 2.26.23. https://mc-stan.org/.

Swofford, D. L. 2002 PAUP*. Phylogenetic Analysis Using Parsimony (*and Other Methods), 4.0 edn, Sinauer, Sunderland, MA.

Tang K., Atkinson B., Smith S. 2020. Cunoniaceae from the Late Cretaceous of North America and its paleobiogeographic implications. Conference Abstract 222, Botany 2020 – Virtual! (Botanical Society of America).

Tang, K., Smith, S., & Atkinson, B. 2022. Extending beyond Gondwana: Cretaceous Cunoniaceae from western North America. *New Phytologist*, 234(2), 704-718.

Tietje M., Antonelli A., Forest F., Govaerts R., Smith S.A., Sun, M., Baker W.J. Eiserhardt W.L. 2023. Global hotspots of plant phylogenetic diversity. *New Phytol*. 240: 1636-1646.

Truswell E.M., Macphail M.K. 2009. Polar forests on the edge of extinction: what does the fossil spore and pollen evidence from East Antarctica say? *Aust. Syst. Bot.* 22:57–106.

Ulloa-Ulloa C., Acevedo-Rodríguez P., Beck S., Belgrano M.J., Bernal R., Berry P.E., Brako L., Celis M., Davidse G., Forzza R.C., Gradstein S.R., Hokche O., León B., León-Yánez S., Magill R.E., Neill D.A., Nee M., Raven P.H., Stimmel H., Strong M.T., Villaseñor J.L., Zarucchi J.L., Zuloaga F.O., Jørgensen P.M. 2017. An integrated assessment of the vascular plant species of the Americas. *Science.* 358:1614–1617.

Van der Hammen T., Werner J., Van Dommelen H.1973. Palynological record of the upheaval of the Northern Andes: A study of the Pliocene and lower quaternary of the Colombian Eastern Cordillera and the early evolution of its high-Andean biota. *Rev. Palaeobot. Palynol*. 16:1–122.

Wang S., Meyer E., McKay J.K., Matz M.V. 2012. 2b-RAD: a simple and flexible method for genome-wide genotyping. *Nat. Methods* 9:808–810.

Wiens J.J., Donoghue M.J. 2004. Historical biogeography, ecology and species richness. *Trends Ecol. Evol.* 19:639-644.

Wilf P., Cúneo N.R., Escapa I.H., Pol D., Woodburne M.O. 2013. Splendid and seldom isolated: the paleobiogeography of Patagonia. Annual Review of Earth and Planetary Sciences 41:561–603.

Willis J. C., H. De Vries H. B. Guppy E. M. Reid, Small J. 1922. Age and area: a study in geographical distribution and origin of species. Cambridge University Press, Cambridge.

Winkworth R.C., Donoghue M.J. 2005. *Viburnum* phylogeny based on combined molecular data: implications for taxonomy and biogeography. *Am. J. Bot.* 92:653-666.

Data available from the Dryad Digital Repository:

https://datadryad.org/stash/share/oByZiKhEUtrkZSA0il4UZ87iem2Gr72GKBScMfX08TU

Statement: During the preparation of this work the author(s) used DeepL Write in order to review the syntax. After using this tool/service, the author(s) reviewed and edited the content as needed and take(s) full responsibility for the content of the published article.

Supplementary Material for:

Phylogeny of *Weinmannia* (Cunoniaceae) reveals the Contribution of the Southern Extratropics to Tropical Andean Biodiversity.

Keywords: immigration, diversification, hyperdiversity, tropics, Gondwana

Index

Supplementary Figures

Supplementary Figure 1: Individual-level 2bRAD-seq tree for Weinmannia. Maximum Likelihood tree inferred from concatenated 2bRAD-seq data from 234 individuals of Weinmannia plus outgroups. Tip labels contain: Specimen_ID# for this study and species name, specimens marked with ** are those selected for species phylogeny. Detailed information for specimens can be found in Appendix 6 (Specimen table). Tips labels are colored by country of origin (see legend). Bootstrap support values are shown as branch labels next to nodes. Accessions from multiple populations of the same morphology-based species form generally well-supported clades except in the case of W. reticulata and W. sorbifolia.

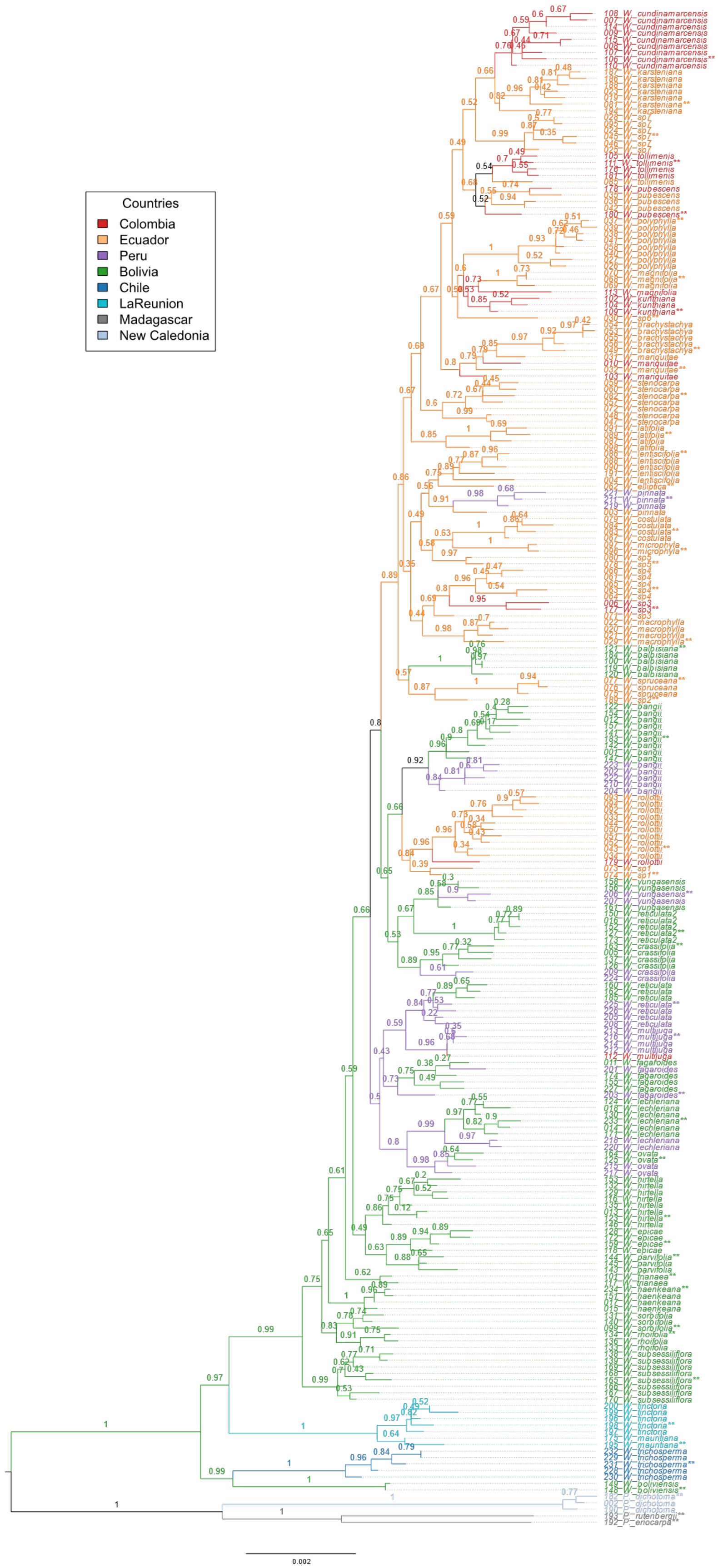
Countries
Colombia
Ecuador
Peru
Bolivia
Chile
LaReunion
Madagascar
New Caledonia
0.002

Supplementary Figure 2. Species-level Phylogeny for Weinmannia. SVDQuartets tree inferred from concatenated 2bRAD-seq data from 48 individuals of *Weinmannia* plus 3 individuals in the outgroup. Bootstrap support values are show as node labels, tip labels and branches are colored by country where species were collected. Branch labels were estimated using RAxML using this topology, (see methods).

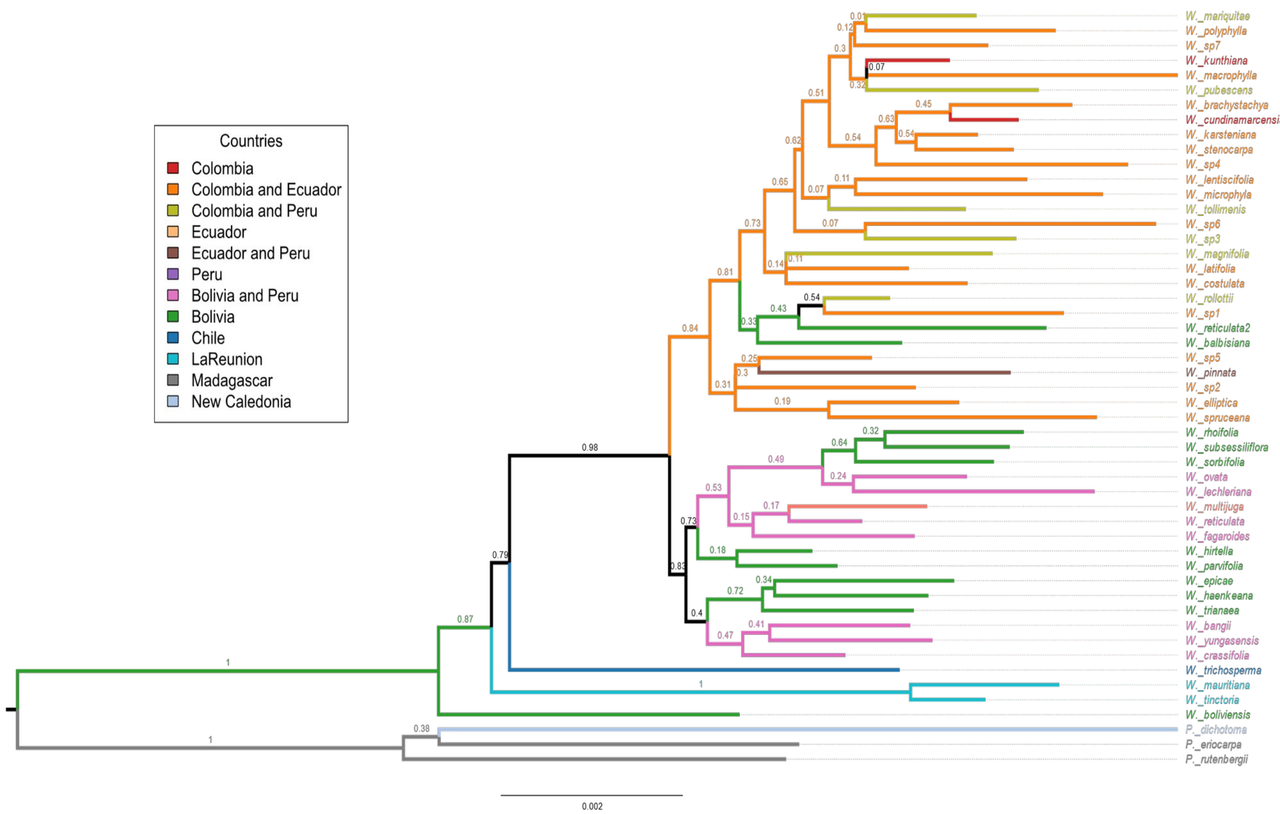

Supplementary Figure 3. Comparison of RAxML and SVDQuartets Species -level trees. *Weinmannia* phylogeny for both methods are compared by highlighting in yellow common spliting patterns. The number of ceros depicted at the nodes trees represent Robinson-Fould distance, among both trees. (Figure generated with TreeDist Package in R)

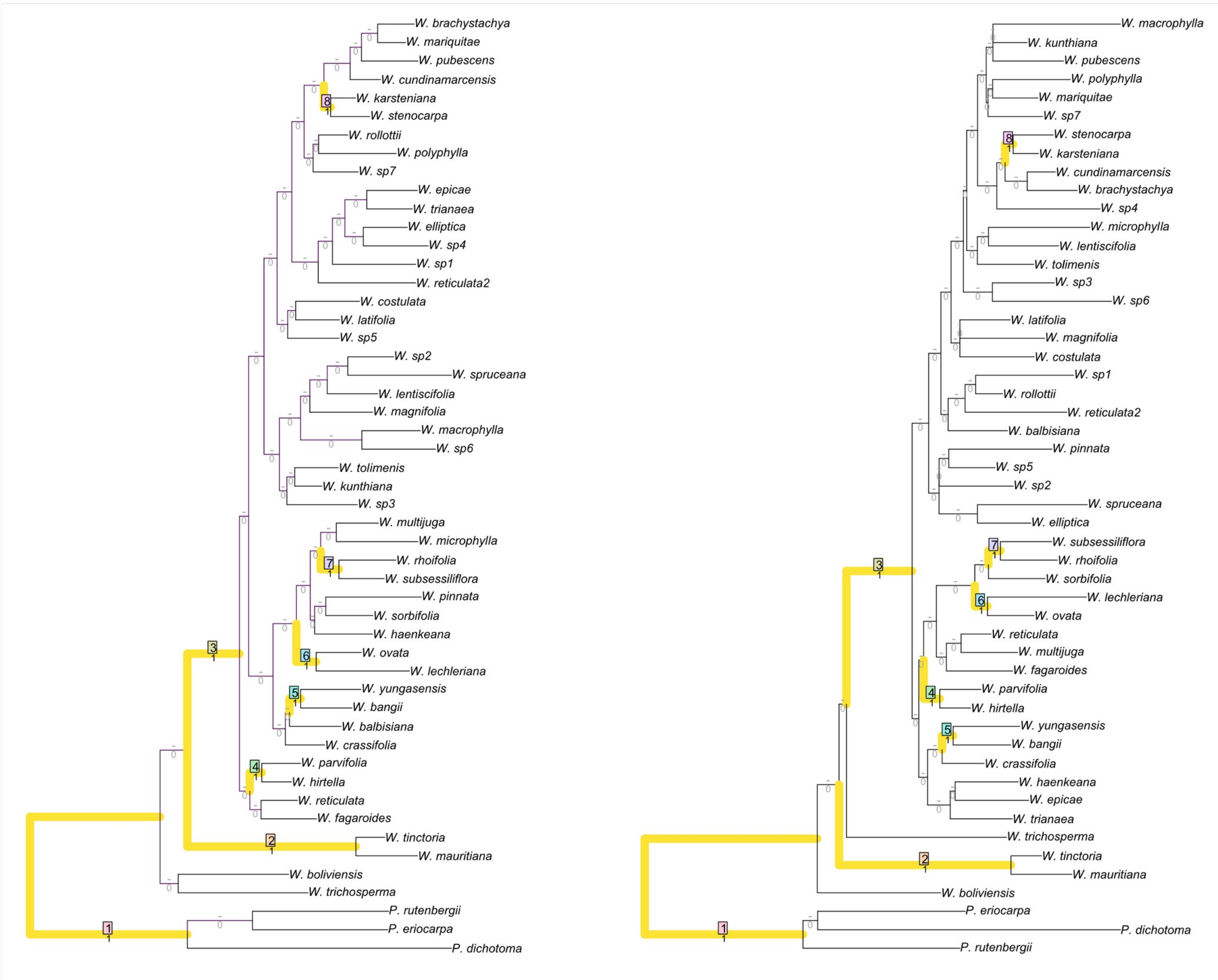

Supplementary Figure 4. SVDQuartets phylogeny with estimated divergence times of *Weinmannia* species. Median divergence age estimates across bootstrap trees with 95% confidence intervals in blue bars (see methods). Time calibration nodes are indicated with stars.

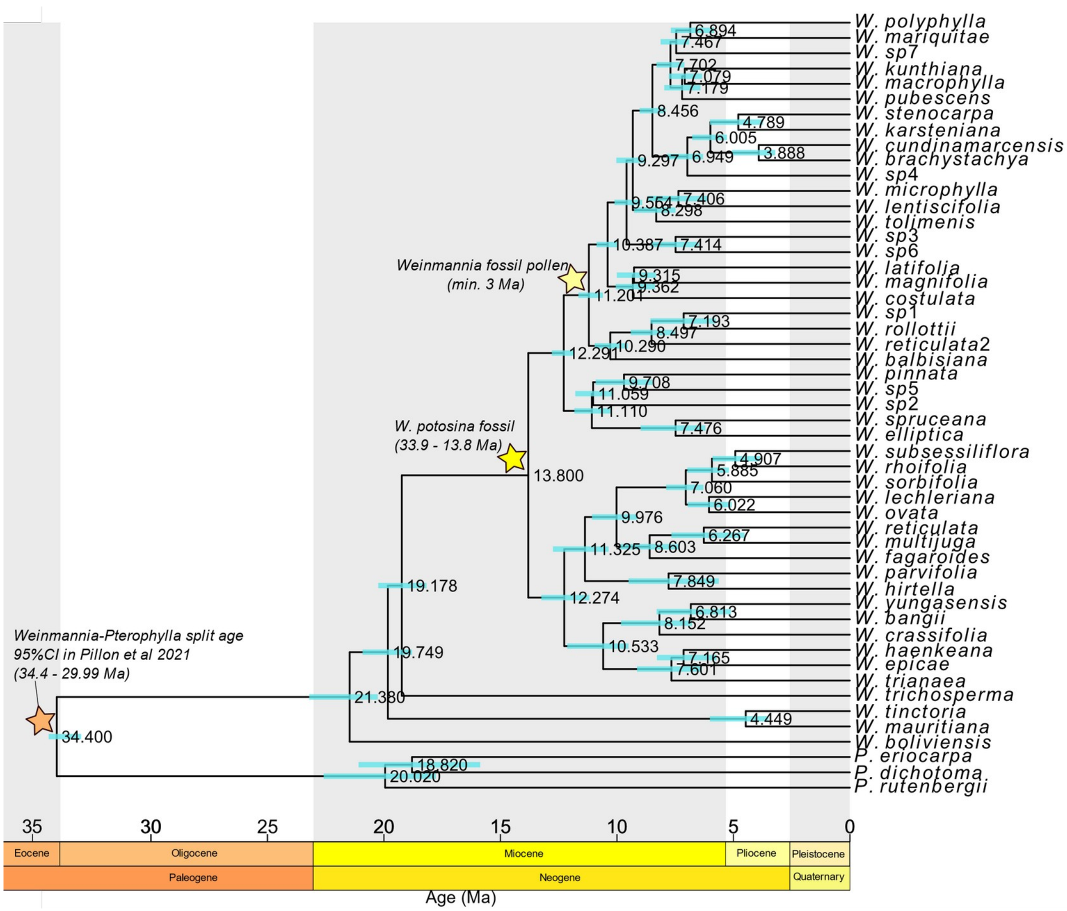

Supplementary Figure 5. Analysis for testing the dispersal from southern latitudes towards the North Andes though the Andes using topology inferred with SVDQuartets excluding Mascarene species. A. Ancestral character estimate for latitude of hypothetical ancestors (nodes). Ancestral states were reconstructed on the SVDQuartets timetree using the minimum latitude of each of the 46 South American *Weinmannia* species considering reviewed accessions. The colors in the figure depict a continuous gradient of latitude, transitioning from southern temperate regions in blue to northern tropical regions in yellow, with intermediate latitudes in the central Andes represented in red. **B. Bayesian linear regression of node age as a function of predicted ancestral latitude: Posterior predictive check.** Observed values are represented in red dots. The blue dots represent the maximum a posteriori estimates, skyblue bars represent 95% High density intervals (HDI). **C. A posteriori probability distribution for the estimated slope coefficient for latitude as a predictor of node age.** Maximum a posteriori (MAP) is equal to β=-0.337and the 95%HDI in blue segment goes from to -0.499 to -0.160 which includes cero, and the 99%HDI goes from -0.555 to -0.0975. This result shows the slope is different from zero (β =0) rejecting the null hypothesis with a 99% of credibility.

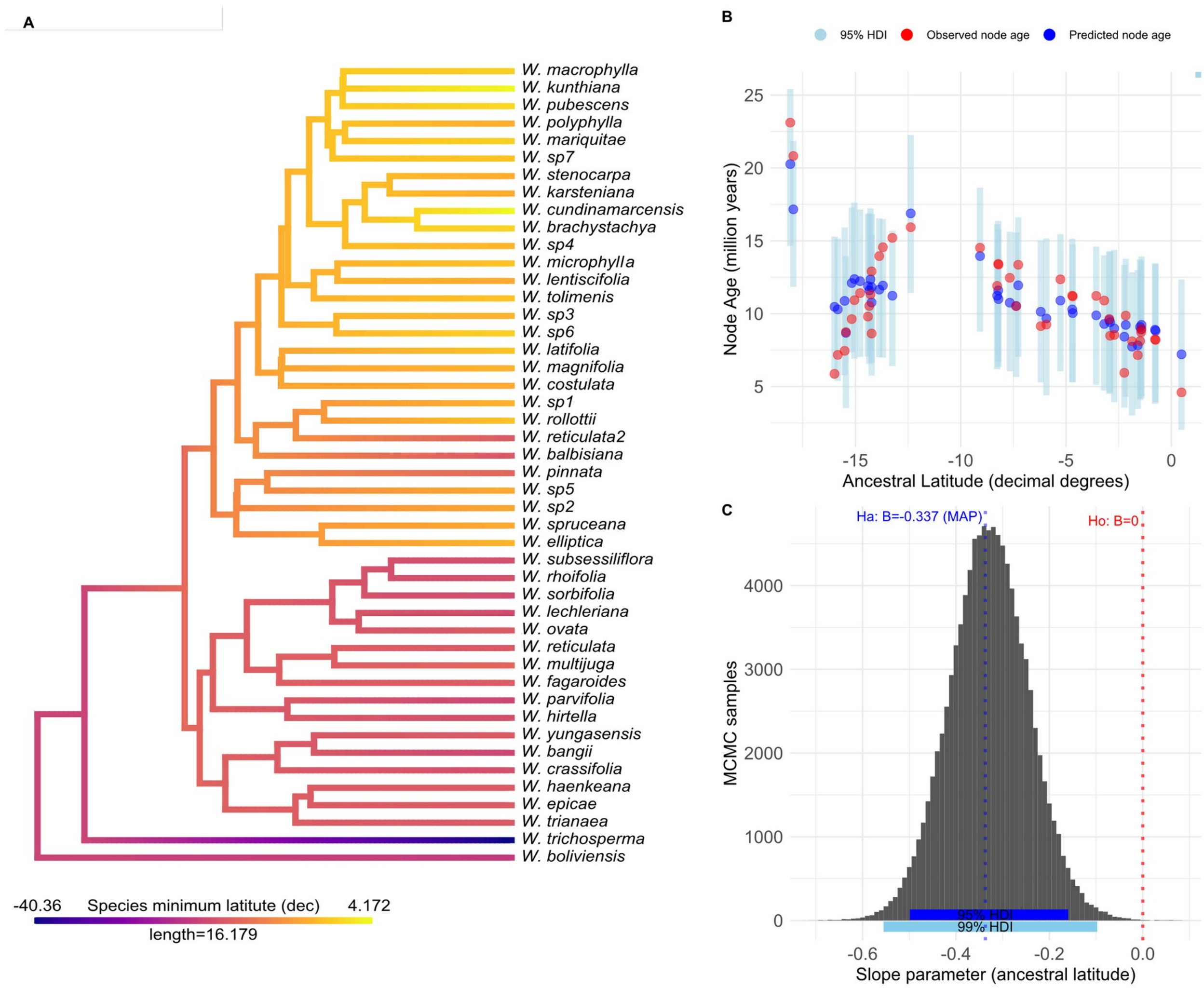

Supplementary Figure 6. Null-Hypothesis test for the slope coefficient when modelling Node Age as a function of ancestral latitude based on non-parametric bootstrap. For each topology inferred and subset analysis performed the blue line indicates the estimated slope coefficient for the linear model predicting node age as a function of ancestral latitude. The density plot indicates the null distribution generated with non-parametric bootstrapping. P-value and slope coefficient ± standard deviation indicated in label next to blue lines. **A.** Test performed using the Maximum likelihood Species-tree excluding Mascarene species. **B.** Test performed using the SVDQuartet Species-tree excluding Mascarene species. **C.** Test performed using the Maximum likelihood Species-tree including all *Weinmannia* species in this study. **D.** Test performed using the SVDQuartet Species-tree including all *Weinmannia* species in this study.

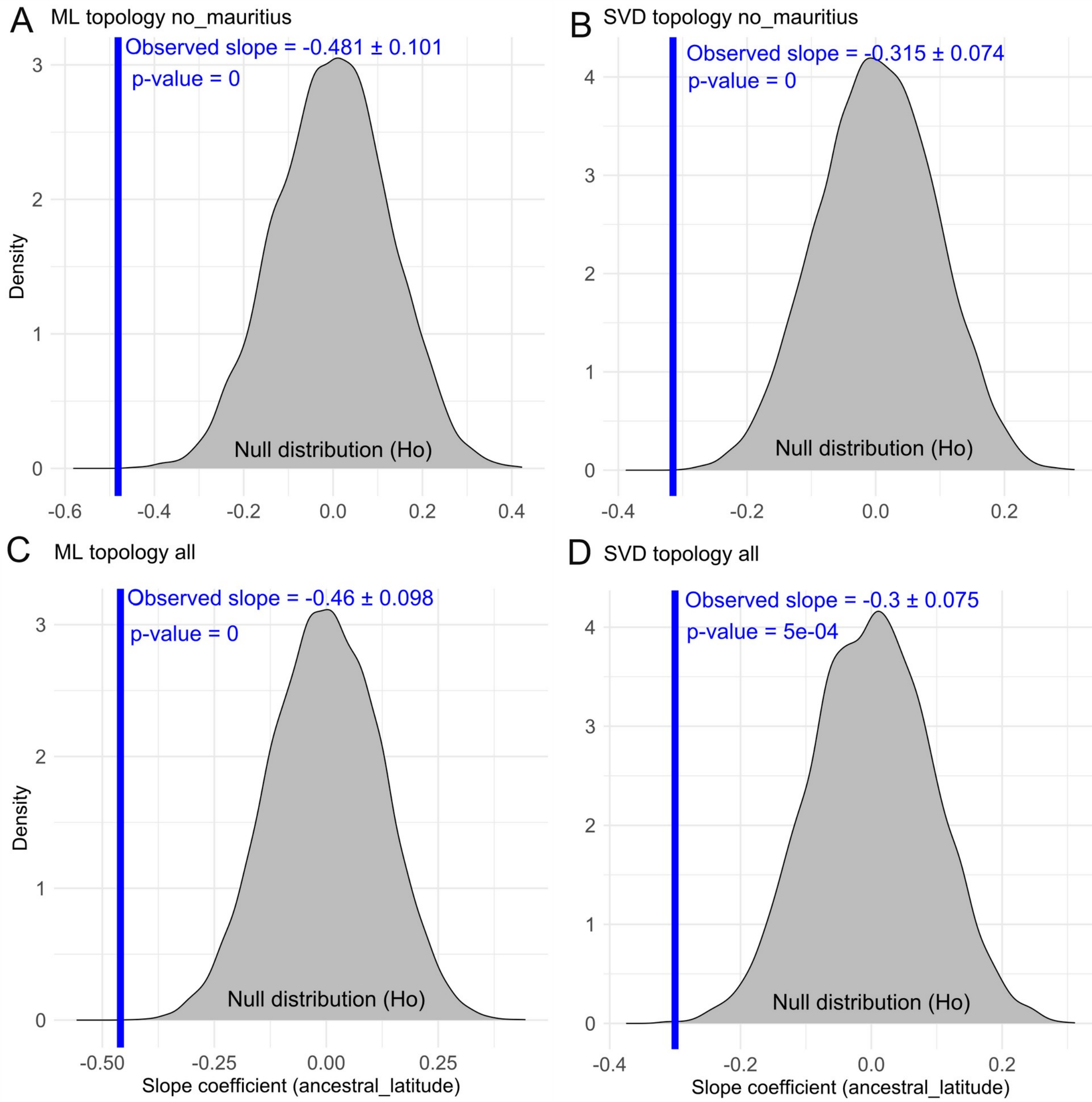

Supplementary Figure 7. Analysis for testing the dispersal from southern latitudes towards the North Andes though the Andes using topology inferred with Maximum Likelihood including Mascarene species. A. Ancestral character estimate for latitude of hypothetical ancestors (nodes). Ancestral states were reconstructed on the Maximum likelihood timetree using the minimum latitude of each of the 48 *Weinmannia* species in this study considering reviewed accessions. The colors in the figure depict a continuous gradient of latitude, transitioning from southern temperate regions in blue to northern tropical regions in yellow, with intermediate latitudes in the central Andes represented in red. **B. Bayesian linear regression of node age as a function of predicted ancestral latitude: Posterior predictive check.** Observed values are represented in red dots. The blue dots represent the maximum a posteriori estimates, skyblue bars represent 95% High density intervals (HDI). **C. A posteriori probability distribution for the estimated slope coefficient for latitude as a predictor of node age.** Maximum a posteriori (MAP) is equal to β=-0.493 and the 95%HDI in blue segment goes from to -0.713 to -0.280, and the 99%HDI goes from -0.778 to -0.207. This result shows the slope is different from zero (β =0) rejecting the null hypothesis with a 99% of credibility.

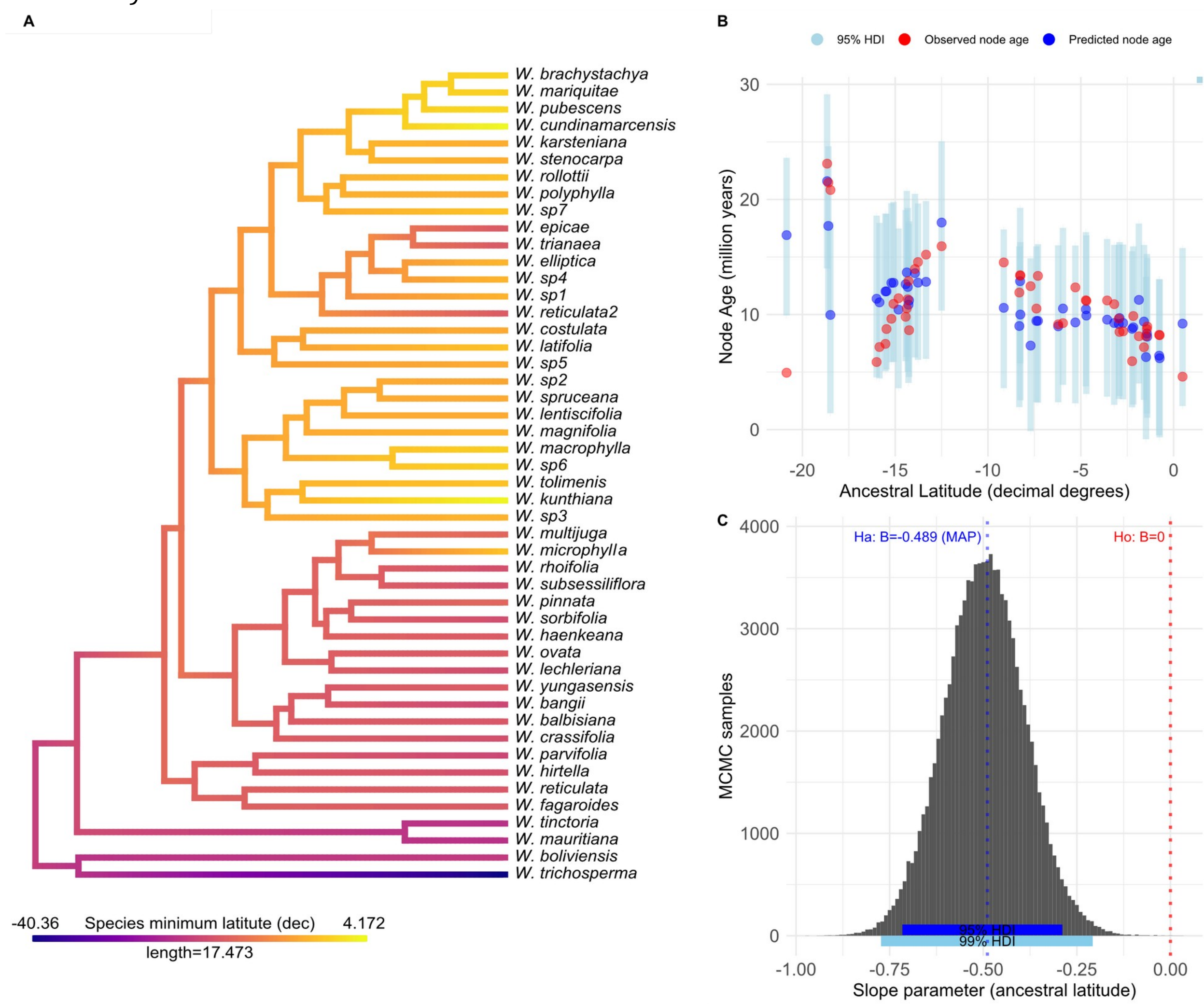

Supplementary Figure 8. Analysis for testing the dispersal from southern latitudes towards the North Andes though the Andes using topology inferred with SVDQuartets including Mascarene species. A. Ancestral character estimate for latitude of hypothetical ancestors (nodes). Ancestral states were reconstructed on the SVDQuartets timetree using the minimum latitude of each of the 48 *Weinmannia* species in this study considering reviewed accessions. The colors in the figure depict a continuous gradient of latitude, transitioning from southern temperate regions in blue to northern tropical regions in yellow, with intermediate latitudes in the central Andes represented in red. **B. Bayesian linear regression of node age as a function of predicted ancestral latitude: Posterior predictive check.** Observed values are represented in red dots. The blue dots represent the maximum a posteriori estimates, skyblue bars represent 95% High density intervals (HDI). **C. A posteriori probability distribution for the estimated slope coefficient for latitude as a predictor of node age.** Maximum a posteriori (MAP) is equal to β=-0.489 and the 95%HDI in blue segment goes from to -0.716 to -0.289, and the 99%HDI goes from -0.773 to -0.208. This result shows the slope is different from zero (β =0) rejecting the null hypothesis with a 99% of credibility.

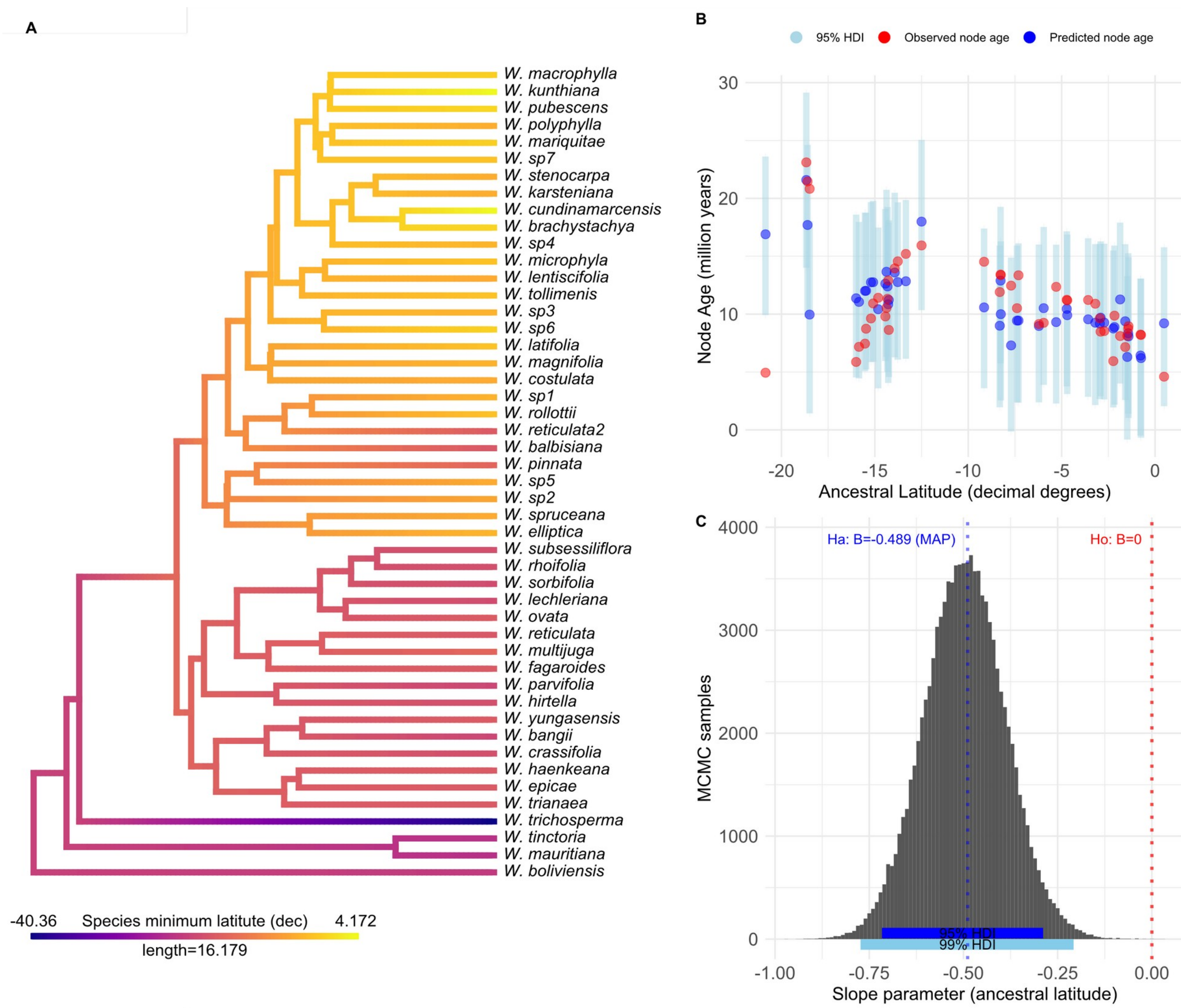

Supplementary Figure 9. Ancestral state reconstruction of 19 climatic variables and elevation under Brownian Motion model for 48 Weinmannia species using out

Maximum likelihood topology. Panels A-S show ancestral character reconstruction for BIO1 to BIO19 and panel T shows the ancestral reconstruction for elevation.

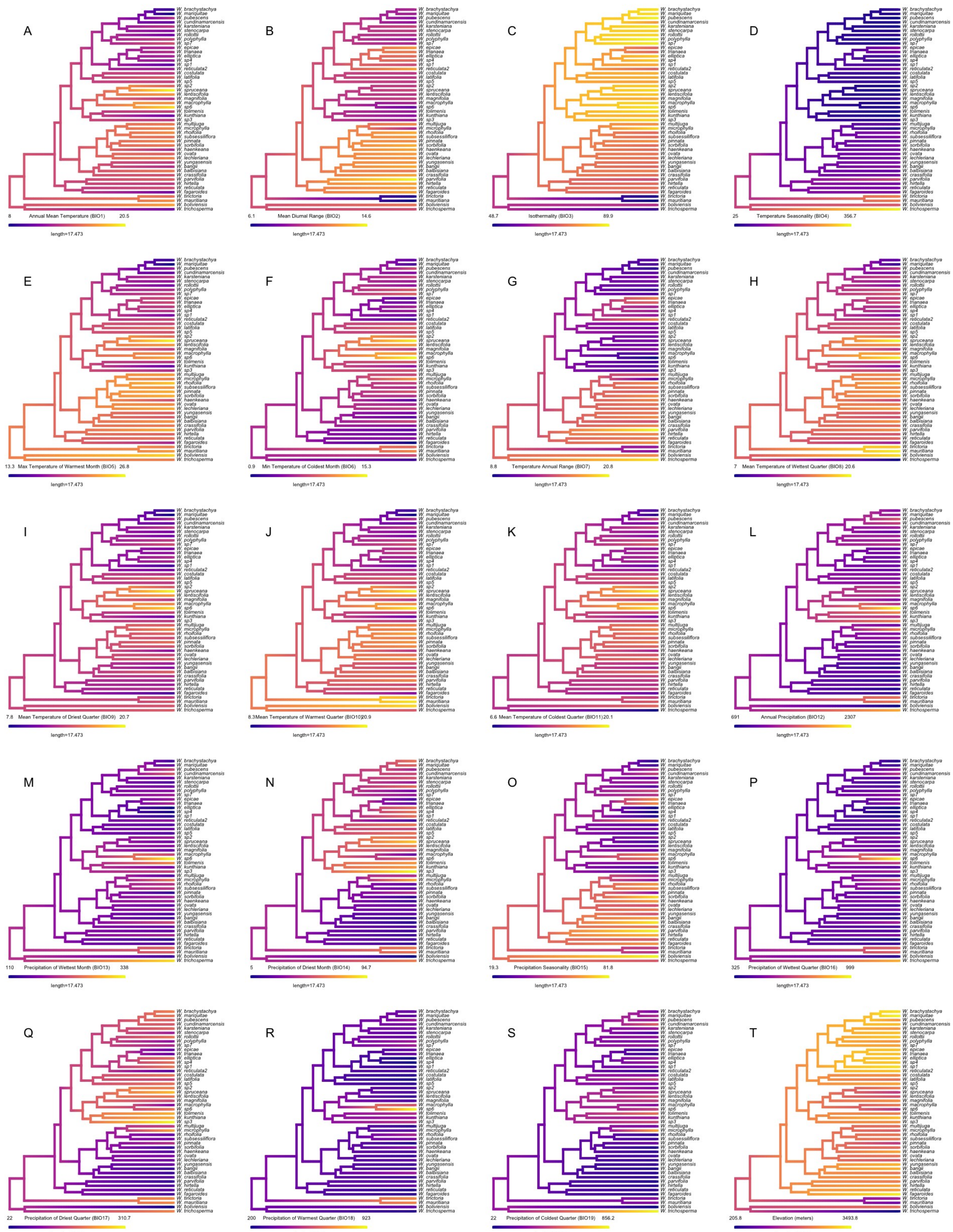

Supplementary Figure 10. Exploratory analysis of climatic niche conservatism and altitudinal niche evolution in relation to latitudinal migration in *Weinmannia*. Scatterplots of evolutionary rates (droot) vs. node depth with fitted linear models (blue curve), slope estimates are indicated in the bottomleft of each plot and the MRCA of the trichosperma-boliviensis clade is marked by a triangle. Colors represent continuous gradients for each variable as indicated in the color scale of each panel: Panels A-K represent Climatic variables that support the hypothesis of niche conservatism as indicated in supplementary figure 1. K represent elevation, M represent latitude.

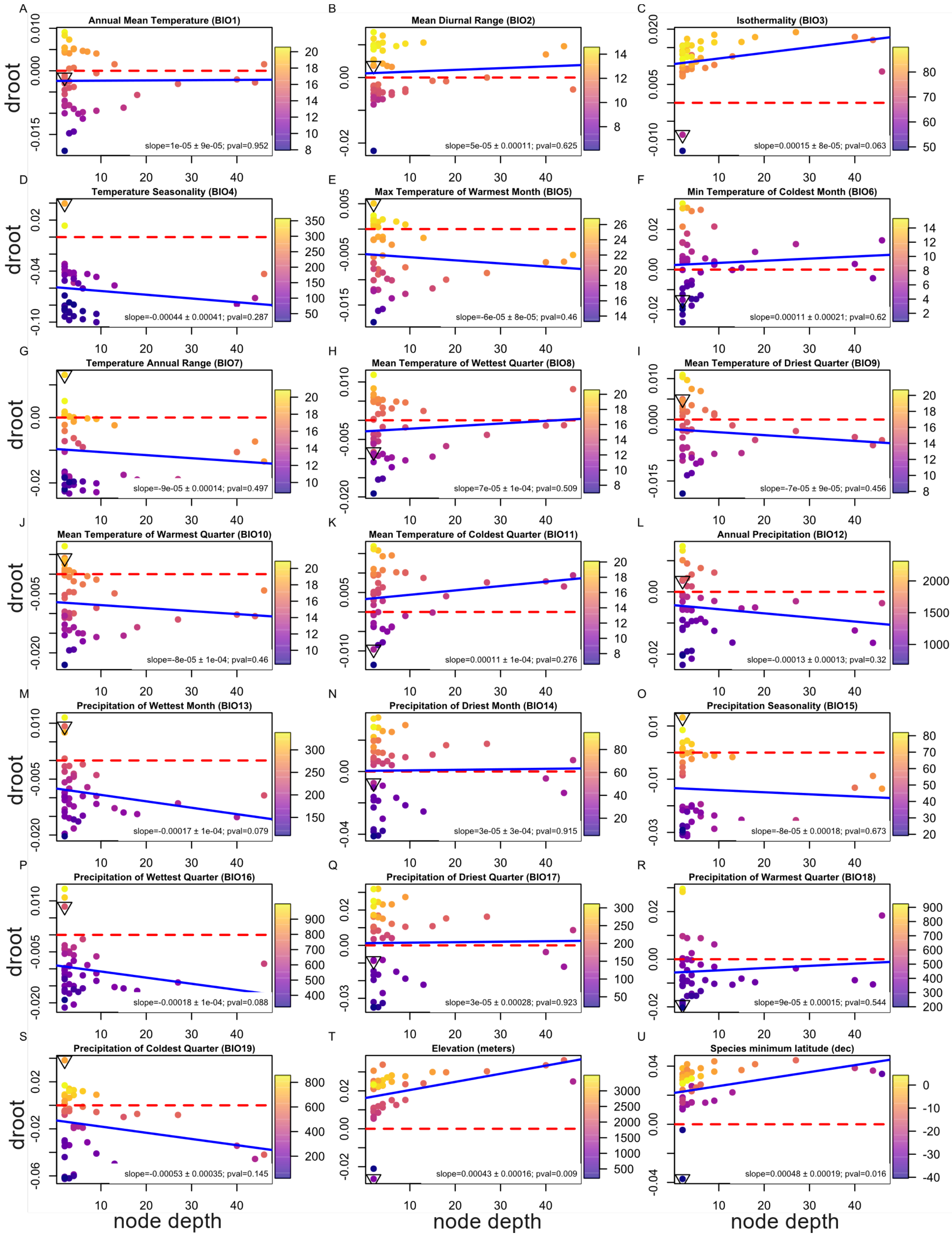
A
Annual Mean Temperature (BIO1)
slope=1e-05 ± 9e-05; pval=0.952
B
Mean Diurnal Range (BIO2)
slope=5e-05 ± 0.00011; pval=0.625
C
Isothermality (BIO3)
slope=0.00015 ± 8e-05; pval=0.063
D
Temperature Seasonality (BIO4)
slope=-0.00044 ± 0.00041; pval=0.287
E
Max Temperature of Warmest Month (BIO5)
slope=-6e-05 ± 8e-05; pval=0.46
F
Min Temperature of Coldest Month (BIO6)
slope=0.00011 ± 0.00021; pval=0.62
G
Temperature Annual Range (BIO7)
slope=-9e-05 ± 0.00014; pval=0.497
H
Mean Temperature of Wettest Quarter (BIO8)
slope=7e-05 ± 1e-04; pval=0.509
I
Mean Temperature of Driest Quarter (BIO9)
slope=-7e-05 ± 9e-05; pval=0.456
J
Mean Temperature of Warmest Quarter (BIO10)
slope=-8e-05 ± 1e-04; pval=0.46
K
Mean Temperature of Coldest Quarter (BIO11)
slope=0.00011 ± 1e-04; pval=0.276
L
Annual Precipitation (BIO12)
slope=-0.00013 ± 0.00013; pval=0.32
M
Precipitation of Wettest Month (BIO13)
slope=-0.00017 ± 1e-04; pval=0.079
N
Precipitation of Driest Month (BIO14)
slope=3e-05 ± 3e-04; pval=0.915
O
Precipitation Seasonality (BIO15)
slope=-8e-05 ± 0.00018; pval=0.673
P
Precipitation of Wettest Quarter (BIO16)
slope=-0.00018 ± 1e-04; pval=0.088
Q
Precipitation of Driest Quarter (BIO17)
slope=3e-05 ± 0.00028; pval=0.923
R
Precipitation of Warmest Quarter (BIO18)
slope=9e-05 ± 0.00015; pval=0.544
S
Precipitation of Coldest Quarter (BIO19)
slope=-0.00053 ± 0.00035; pval=0.145
T
Elevation (meters)
slope=0.00043 ± 0.00016; pval=0.009
U
Species minimum latitude (dec)
slope=0.00048 ± 0.00019; pval=0.016
droot
node depth

Supplementary Table 1. Significance test assessing whether the estimated mean evolutionary rates (droot) deviate from the background rate under the linear model: abs(droot) ~ variable - 1. Displayed are the population mean absolute droot estimates (Intercept coefficients), standard errors, and Wald test statistics (Chi-square, degrees of freedom, and p-value). White rows: droot values do not differ from the background rate (p > 0.01). Light blue rows: droot values are lower than the background rate (p<0.01). Red rows: droot values are higher than the background rate (p<0.01).

Variable	Esimated mean	Error	Chi-square	df	p-value
Annual Mean Temperature (BIO1)	0.00589	0.00141	39.2948	1	0.0000
Mean Diurnal Range (BIO2)	0.00664	0.00141	32.9569	1	0.0000
Isothermality (BIO3)	0.01251	0.00140	2.4949	1	0.1199
Temperature Seasonality (BIO4)	0.06255	0.00133	1290.7253	1	0.0000
Max Temperature of Warmest Month (BIO5)	0.00635	0.00141	35.3443	1	0.0000
Min Temperature of Coldest Month (BIO6)	0.01244	0.00140	2.6673	1	0.1132
Temperature Annual Range (BIO7)	0.01132	0.00140	5.8953	1	0.0199
Mean Temperature of Wettest Quarter (BIO8)	0.00643	0.00141	34.6851	1	0.0000
Mean Temperature of Driest Quarter (BIO9)	0.00611	0.00141	37.3659	1	0.0000
Mean Temperature of Warmest Quarter (BIO10)	0.00855	0.00141	19.2706	1	0.0000
Mean Temperature of Coldest Quarter (BIO11)	0.00710	0.00141	29.3724	1	0.0000
Annual Precipitation (BIO12)	0.00877	0.00140	17.9604	1	0.0000
Precipitation of Wettest Month (BIO13)	0.00998	0.00140	11.4115	1	0.0011
Precipitation of Driest Month (BIO14)	0.01832	0.00139	6.6706	1	0.0137
Precipitation Seasonality (BIO15)	0.01538	0.00140	0.2208	1	0.6384
Precipitation of Wettest Quarter (BIO16)	0.01167	0.00140	4.7497	1	0.0362
Precipitation of Driest Quarter (BIO17)	0.01705	0.00139	2.7866	1	0.1109
Precipitation of Warmest Quarter (BIO18)	0.00976	0.00140	12.5320	1	0.0006
Precipitation of Coldest Quarter (BIO19)	0.02310	0.00138	36.5943	1	0.0000
Elevation (meters)	0.02117	0.00139	21.5928	1	0.0000
Species minimum latitude (dec)	0.02651	0.00138	72.9664	1	0.0000

Supplementary Methods

Supplementary Methods 1 – Bayesian regression. Bayesian regression analysis. We developed a hierarchical Bayesian regression to assess correlation structures from nesting patterns between phylogenetic nodes, considering evolutionary relationships in latitude observations. The model, implemented in Stan v. 2.18.2 (Carpenter et al. 2017) via Hamiltonian MCMC, was run in R using the rstan package v. 2.26.23 (Stan Development Team 2023). Full Stan code is provided in Supplementary Materials 1. The linear predictor function is defined as:

$$\mu_{n\,=} = \alpha_{int} + \beta * X_n + \theta_n \qquad (1)$$

Where μ_n is the linear predictor for the expected node age Y_n for each observation at node n, α_{int} is the intercept, X_n is the estimated ancestral latitude, β is the slope representing the change in Y for a one-unit change in X, and θ_n is the random effect for each node capturing unexplained variation. Random effects were drawn from a multivariate normal distribution, accounting for correlations from shared evolutionary history according to the following function:

$$\theta n \sim multinormal(0_N, \Sigma) \qquad (2)$$

Where 0_N is a zero-mean vector of length N (the number of nodes) and Σ is the phylogenetic covariance matrix. We generated this matrix using the makeL1 function from the RRphylo package in R (Castiglione et al. 2018), which constructs an NxN matrix of branch lengths for all root-to-node paths, capturing hierarchical relationships between node pairNode age Yn was modeled as a likelihood function with normally distributed error with mean drawn from μ_n as follows:

$$Yn \sim normal(\mu_n, \varepsilon_n) \qquad (3)$$

Where ε_n is the residual standard deviation, capturing unexplained variation in Y after accounting for X and random effects (θ). The model was fitted using four independent MCMC chains, each running 3,000,000 iterations. For efficiency, chains were thinned every 10 iterations, yielding 300,000 samples per chain, with the first 50,000 discarded as burn-in. The max_treedepth was set to 10 to address divergent transitions during sampling.

Supplementary Methods 2 – Exploratory analysis of thermal niche conservatism. To support our hypothesis of Weinmannia's south-to-north migration with an extratropical origin, we assessed thermal niche conservatism across the phylogeny. We performed ancestral reconstructions of mean annual temperature (BIO1) and elevation using a time-calibrated ML species-level phylogeny. BIO1 values were extracted from WorldClim 2 (Fick & Hijmans 2017) at a 0.5 arc-second resolution, and elevation was estimated from geo-referenced herbarium specimen data.

To evaluate trait conservatism, we used a color gradient to map observed and reconstructed values onto the species-tree edges using the 'contMap' function in phytools v.2.1, under a Brownian motion model. We assessed whether ancestral values at basal nodes were retained throughout the tree by calculating the Darwin (*d*) rate of trait evolution per unit time (Haldane 1949) for each node using reconstructed values of BIO1 to BIO19, Elevation, and Latitude. The rate of change from each node to the root node (putative extratropical ancestor) was calculated as d_{root}. As follows:

$$d_{root} = [\ln(X_i) - \ln(X_{root})] / \Delta time) \qquad (4)$$

Where X_i was the estimated value for each *i* node and X_{root} was the estimated value of that same trait for the root node, the MRCA of all *Weinmannia*. *Δtime* is the distance in million years from the root node to the *i* node. To statistically assess if d_{root} differed significantly between the reconstructed traits (BIO1, Elevation, and Latitude), we employed a generalized linear model (GLM) framework fitting a Gaussian GLM without an intercept, allowing the mean absolute d_{root} to be estimated independently for each trait as follows:

$$d_{root} \sim trait - 1 \qquad (5)$$

The resulting coefficients represent the mean d_{root} for each group (BIO1 to BIO19, Elevation, and Latitude). We used Wald tests implemented in the R package aod to determine if the mean d_{root} for each group was significantly different from the background (mean) droot across all variables zero. Estimated values statistically lower or equal to the background were taken as evidence for conservatism of the ancestral values across nodes. Additionally, we performed pairwise t-tests to compare the means of absolute d_{root} between each trait group.

References Supplementary Methods

Carpenter B., Gelman A., Hoffman M.D., Lee D., Goodrich B., Betancourt M., Brubaker M., Guo J., Li P., Riddell A. 2017. Stan: A Probabilistic Programming Language. *J. Stat. Soft*. 76:1–32.

Castiglione S., Tesone G., Piccolo M., Melchionna M., Mondanaro A., Serio C., Di Febbraro M., Raia P. 2018. A new method for testing evolutionary rate variation and shifts in phenotypic evolution. *Methods in Ecology and Evolution* 9:974–983.

Haldane, J.B.S., 1949. Suggestions as to Quantitative Measurement of Rates of Evolution. Evolution 3, 51–56.

Stan Development Team. 2023. RStan: the R interface to Stan. R package version 2.26.23. https://mc-stan.org/.